

2014

# Investigating the role of Dachshund Homolog 1 (DACH1) and miR-200b in Group 4 medulloblastoma pathogenesis

Courtney George  
*Edith Cowan University*

---

## Recommended Citation

George, C. (2014). *Investigating the role of Dachshund Homolog 1 (DACH1) and miR-200b in Group 4 medulloblastoma pathogenesis*. Retrieved from [https://ro.ecu.edu.au/theses\\_hons/191](https://ro.ecu.edu.au/theses_hons/191)

This Thesis is posted at Research Online.  
[https://ro.ecu.edu.au/theses\\_hons/191](https://ro.ecu.edu.au/theses_hons/191)

# Edith Cowan University

## Copyright Warning

You may print or download ONE copy of this document for the purpose of your own research or study.

The University does not authorize you to copy, communicate or otherwise make available electronically to any other person any copyright material contained on this site.

You are reminded of the following:

- Copyright owners are entitled to take legal action against persons who infringe their copyright.
- A reproduction of material that is protected by copyright may be a copyright infringement.
- A court may impose penalties and award damages in relation to offences and infringements relating to copyright material. Higher penalties may apply, and higher damages may be awarded, for offences and infringements involving the conversion of material into digital or electronic form.

### **Use of Thesis**

This copy is the property of Edith Cowan University. However the literary rights of the author must also be respected. If any passage from this thesis is quoted or closely paraphrased in a paper or written work prepared by the user, the source of the passage must be acknowledged in the work. If the user desires to publish a paper or written work containing passages copied or closely paraphrased from this thesis, which passages would in total constitute an infringing copy for the purpose of the Copyright Act, he or she must first obtain the written permission of the author to do so.

**Investigating the role of Dachshund Homolog 1  
(DACH1) and miR-200b in Group 4  
medulloblastoma pathogenesis**

---

Honours, 2014

Courtney George

Edith Cowan University

Primary Supervisor: Dr Peter Dallas, Telethon Kids Institute

Secondary Supervisor: Professor Mel Ziman, Edith Cowan University

**I.**

**COPYRIGHT AND ACCESS DECLARATION**

I certify that this thesis does not, to the best of my knowledge and belief:

- (i) incorporate without acknowledgment any material previously submitted for a degree or diploma in any institution of higher education;
- (ii) contain any material previously published or written by another person except where due reference is made in the text; or
- (iii) contain any defamatory material

Signed ..... Courtney George .....

Dated ..... 3<sup>rd</sup> November, 2014 .....

## II.

### ABSTRACT

Medulloblastoma is the most common malignant childhood brain tumour, and the most significant cause of childhood cancer-related mortality. Recently four core molecular medulloblastoma sub-groups have been identified, with distinct pathogenesis and responses to therapies. Current therapies, do not account for this molecular variation, and many patients may receive inappropriate treatment. To address this, targeted therapies for each molecular sub-group would be ideal. Unfortunately, for the more aggressive Group 3 and Group 4 sub-groups, the underlying mechanisms of pathogenesis remain poorly understood. The current challenge is to identify the key tumour suppressors or oncogenes involved in Group 3 and Group 4 pathogenesis, which may ultimately lead to the development of new therapeutic targets.

Transcriptional profiling studies of medulloblastoma have identified numerous genes commonly affected in other cancers, which may also contribute to medulloblastoma pathogenesis. One potential candidate is Dachshund Homolog 1 (DACH1), which has up-regulated expression across all medulloblastoma sub-groups, relative to normal cerebellum, consistent with a potential oncogenic role. This up-regulation is most significant in the Group 4 tumours and is consistent with recent methylation profiling analyses, correlating increased DACH1 expression with gene hypomethylation. This combined evidence suggests that DACH1 may be a medulloblastoma oncogene. Oncogenic over-expression of DACH1 has been demonstrated in both ovarian and colorectal cancers, and is associated with cancer progression and invasiveness, but has not previously been linked to medulloblastoma pathogenesis. Additionally the mechanisms associated with over-expression of DACH1 have not been explored in any cancers; however epigenetic modulation is likely, as DACH1 mutations are relatively rare in most cancer types, and DACH1 mutations in medulloblastoma have not been identified.

Deregulated expression of numerous microRNAs has been identified in various cancers, including medulloblastoma, demonstrating the role of microRNAs in cancer initiation and progression. MicroRNAs provide a potential epigenetic mechanism for regulation of

DACH1. Analysis of the DACH1 3'UTR using TargetScan revealed a potential binding sites for nine individual/clusters of miRNAs (Figure 10). One putative miRNA is miR-200b, belonging to the highly conserved microRNA-200 family (miR-200). miR-200 is frequently down-regulated in metastatic cancers, raising the possibility that the miR-200 family may play a role in the pathogenesis of metastatic Group 4 medulloblastoma.

There is an apparent association between high levels of DACH1 expression and low level of miR-200b, and *in silico* analysis using TargetScan identified a putative binding site for miR-200b within the DACH1 3'-UTR at nucleotides 971-978. Previous evidence supports the role of both DACH1 and miR-200b in metastatic progression; however an association between the two has not previously been described. Here we propose that deregulated DACH1 was associated with loss of regulation by miR-200b, and demonstrated an inverse correlation between DACH1 and mir-200b expression in representative medulloblastoma cell lines, which was further assessed.

### III.

## TABLE OF CONTENTS

I	COPYRIGHT AND ACCESS DECLARATION	
II	ABSTRACT.....	1
III	TABLE OF CONTENTS.....	3
IV	LIST OF FIGURES.....	6
V	LIST OF TABLES.....	8
VI	ACKNOWLEDGEMENTS.....	9
VII	APPENDICES	
1.0	MEDULLOBLASTOMA.....	10
1.1	The four core medulloblastoma sub-groups.....	11
1.2	Group 3 and Group 4 medulloblastoma.....	15
1.3	Potential mechanisms involved in Group 3 and Group 4 medulloblastoma pathogenesis.....	16
2.0	DACHSHUND HOMOLOG 1.....	18
2.1	DACH1 as a tumour suppressor.....	18
2.2	DACH1 as an oncogene.....	20
2.3	DACH1 expression in medulloblastoma.....	21
2.4	Regulation of DACH1 expression.....	22
3.0	MicroRNA.....	23
3.1	microRNA and cancer.....	24
3.2	microRNA and medulloblastoma.....	25
3.3	Epithelial-mesenchymal transition (EMT).....	27
3.3.1	miRNAs, EMT, and metastasis.....	27
3.3.2	The miR-200 family and miR-200b in EMT.....	28

4.0	SUMMARY .....	32
4.1	Aims .....	33
5.0	METHODS .....	34
5.1	Cell culture .....	34
5.1.1	Countess: Cell number and viability .....	35
5.2	Protein extraction .....	36
5.3	SDS Polyacrylamide gel electrophoresis (SDS-PAGE) and immunoblotting .....	36
5.4	Extraction of total RNA .....	37
5.5	TaqMan® Gene Expression assay .....	38
5.6	TaqMan® microRNA assay .....	39
5.7	Lentiviral transductions .....	40
5.8	Cloning .....	43
5.8.1	Transformation of <i>E.Coli</i> .....	43
5.9	Generation of Lentivirus .....	44
5.10	Transfection .....	45
5.10.1	Lipofectamine® RNAiMAX lipofectamine transfection .....	46
5.10.2	Tali™ Image based cytometer .....	47
5.11	Data Analysis .....	47
5.11.1	qRT-PCR expression data .....	47
5.11.2	Western blot and protein quantitation .....	48
6.0	RESULTS .....	49
6.1	An inverse correlation between DACH1 and miR-200b expression in medulloblastoma cell lines .....	49
6.2	Addressing the inverse correlation between DACH1 and miR-200b .....	53
6.2.1	Stable transductions with lentivirus .....	53
6.2.2	Transient transfection of selected medulloblastoma cell lines .....	53
6.2.3	Confirming miR-200b expression post-transfection .....	54
6.2.4	Determining inhibition of DACH1 by miR-200b .....	55
6.2.5	Optimising transient transfection of adherent medulloblastoma cell lines .....	55

7.0	DISCUSSION.....	66
7.1	DACH1 and miR-200b expression are inversely correlated in medulloblastoma cell lines.....	66
7.2	Stable lentiviral transduction to generate reporter cell lines.....	68
7.3	Transient transfection to alter miR-200b levels.....	68
7.4	TaqMan® qRT-PCR assays.....	70
7.5	Additional consideration.....	71
8.0	CONCLUSION.....	72
9.0	REFERENCES.....	73

## IV.

### LIST OF FIGURES

- Figure 1. Sonic Hedgehog (SHH) and Wingless (WNT) signalling pathways**
- Figure 2. Distribution of sub-group specific survival, occurrence, and metastasis**
- Figure 3. Mechanisms of DACH1-mediated inhibition of epithelial-mesenchymal transition (EMT)**
- Figure 4. DACH1 expression across all sub-groups**
- Figure 5. The typical miRNA biogenesis pathway**
- Figure 6. The normal and abnormal behaviour of miRNAs**
- Figure 7. miRNA expression in EMT**
- Figure 8. The miR-200 family members have two conserved seed sequences**
- Figure 9. Simplified overview of the regulatory role of miR-200b in EMT**
- Figure 10a. TargetScan putative miRNA binding sites**
- Figure 10b. miR-200 family seed sequence interaction with DACH1 3'UTR**
- Figure 11a. DACH1-3'UTR-GFP-Lenti reporter viral vector**
- Figure 11b. lenti-miRa-GFP-hsa-miR-200b viral vector**
- Figure 11c. pLenti-III-blank-lentiviral vector**
- Figure 12. pLenti-DACH1-3'UTR-Luc reporter vector**
- Figure 13. Expression of DACH1 and miR-200b in medulloblastoma cell lines, relative to D283.**
- Figure 14. DACH1 protein expression in six representative medulloblastoma cell lines with quantitative analysis of protein expression**

- Figure 15.** Successful transient transfection of cell lines with 20nM and 50nM of hsa-mir-200b-3p mimic, confirmed by qRT-PCR
- Figure 16.** DACH1 mRNA expression is not affected by miR-200b expression in cells transiently transfected with 20nM of miR-200b mimic, at 24 hours and 48 hours post-transfection.
- Figure 17.** DACH1 protein expression does not appear to be translationally repressed in cells transiently transfected with 20nM of miR-200b mimic, compared to cells transfected with 20nM of control, at 24 and 48 hours post-transfection
- Figure 18.** DACH1 mRNA expression is not affected by miR-200b in cells transiently transfected with 50nM hsa-mir-200b-3p mimic at 24 hours post-transfection.
- Figure 19.** DACH1 protein expression does not appear to be translationally repressed in cells transiently transfected with 50nM of miR-200b mimic, compared to un-transfected cells, at 24 hours post-transfection

## V.

### LIST OF TABLES

- Table 1.** Summary of key features of the four core medulloblastoma sub-groups
- Table 2.** Cell culture conditions
- Table 3.** Simplified summary: an inverse correlation exists between DACH1 and miR-200b

## VI.

### ACKNOWLEDGEMENTS

I would like to take this opportunity to thank everyone who assisted in the production of this thesis. First of all to my supervisor Dr Peter Dallas, for allowing me to be part of such a challenging and rewarding project. Thank you for everything, especially your patience and guidance throughout the year. I don't think I could have picked a better supervisor to learn from. Thank you also to my Co-supervisor, Professor Mel Ziman, your encouraging words and help throughout were very much appreciated!

To everyone in the Brain Tumour team, especially Hillary, there were many issues I could not have overcome without your help and advice. My fellow honours buddies, thanks for sharing the experience, and all the late nights in the lab with me!

The biggest thank you to my family, especially my sister Tenielle, for taking on the role as my own personal editor and audience, and helping me out even when you didn't want to. I don't know what I would have done without your help. Also to my mum and dad for always having faith in me and being proud no matter what. I doubt I would be where I am today without any of you.

Finally, I would like to acknowledge the scholarship funding provided by the Cancer Council of Western Australia, and the Telethon Adventurers.

## 1.0 MEDULLOBLASTOMA

Medulloblastoma is the most common malignant brain tumour in children, and occurs in the cerebellum. The clinical heterogeneity of these tumours has now been linked to variations at a molecular level, distinguishing at least four distinct sub-groups. These core sub-groups include the Sonic Hedgehog tumours (SHH), Wingless tumours (WNT), Group 3 tumours, and Group 4 tumours. For SHH and WNT tumours, aberrant overexpression of the respective pathways is responsible for driving tumourigenesis. However, the pathogenesis of both Group 3 and Group 4 tumours is more complex, most likely involving interactions between different signalling and genetic factors. In Group 3, MYC amplification is the most striking abnormality, and in Group 4, recurrent mutations affecting epigenetic regulator genes are prominent.

Given the molecular and clinical heterogeneity of medulloblastoma, it would be ideal to treat patients according to molecular sub-group, however current treatment regimens are determined using a risk stratification that classifies patients as either high risk or low risk - high risk being those aged  $\geq 3$  years at diagnosis, with metastatic dissemination and/or  $\geq 1.5\text{cm}^2$  residual tumour following surgical resection, or  $< 3$  years of age at diagnosis, and those of average risk being  $\geq 3$  years of age at diagnosis, without metastatic dissemination, and  $\leq 1.5\text{cm}^2$  residual tumour following surgical resection (DeSouza, Jones, Lowis, & Kurian, 2014; Klesse & Bowers, 2010; Pizer & Clifford, 2008). Patients receive a combination of therapies, depending on 'risk', including surgical resection, craniospinal radiation, and a combination of chemotherapeutic agents (Wlodarski & Jozwiak, 2008). While the use of combination therapy has greatly improved patient survival, serious long-term post-treatment related health issues are common due to the aggressive nature of treatment. Given the current risk-based approach (for determining treatment) does not account for the molecular heterogeneity and the variability in outcome associated with each sub-group, some patients may receive inadequate treatment, while others receive unnecessarily aggressive treatment. This highlights the importance of a therapeutic approach based on molecular sub-group and patient prognosis (Northcott et al., 2011), and the need to develop therapies that are sub-group specific.

SHH and WNT pathway inhibitors have been developed and some are currently utilised in the clinic for cancer treatment. Such targeted therapies would be appropriate in treating medulloblastoma, given the variation in tumour responsiveness to current therapies. Particularly for the WNT sub-group patients, which have an excellent prognosis and are likely to be ‘over-treated’ using current risk stratification, patients would greatly benefit from less aggressive therapies that produce less detrimental side effects. In brain tumours, several clinical trials of drugs targeting multiple components of the WNT signalling pathway are currently underway (MacDonald, Aguilera, & Castellino, 2014). Additionally, the SMO inhibitor; vismodegib (GDC-0449), is an FDA approved treatment for basal cell carcinoma that is currently being trialled for SHH medulloblastoma (DeSouza et al., 2014; MacDonald et al., 2014; Remke, Ramaswamy, & Taylor, 2013). The effectiveness of such therapies in medulloblastoma would be a major step towards improving patient outcome. Unfortunately for the more complex and aggressive Group 3 and Group 4 tumours, no such targeted therapies exist. However, a more comprehensive understanding of the molecular pathogenesis will likely identify new potential therapeutic targets, and enable the future development of successful therapies that will improve medulloblastoma patient outcome.

## **1.1 The four core medulloblastoma sub-groups**

It is important to understand the heterogeneity of medulloblastoma tumours at the clinical level, as well as at the molecular level. An overview of clinical and molecular features of each of the sub-groups is presented in Table 1. The recognition that distinct genetic profiles exist amongst medulloblastoma tumours, has galvanised research in the field and revolutionised the understanding of medulloblastoma pathogenesis, identifying at least four core molecular sub-groups. Together, transcriptome, mutation, and cytogenetic analyses have identified sub-group specific alterations, and presented numerous candidate tumour suppressors and oncogenes for each sub-group that required additional analysis.

To elaborate on these sub-groups; both SHH and WNT medulloblastoma tumours are linked to over-activation of the respective signalling pathways, with numerous mutations being implicated in tumour development (Remke et al., 2013; Taylor et al., 2012). Both are relatively well characterised with a clear understanding of the mechanisms involved in tumourigenesis (for review, see (Huse & Holland, 2010)). Over-activation of either of these

pathways is sufficient in tumour initiation, and is the result of mutations to intermediates along the respective signalling pathways (Figure 1). Inactivation mutations to *Suppressor of Fused (SUFU)* or *Patched receptor (PTCH1)*, or activation mutations of *Smoothened (SMO)*, constitutively activate the sonic hedgehog signalling pathway with consequent over-expression of target oncogenes such as MYC family oncogenes (Huse & Holland, 2010; Jones et al., 2012; Northcott, Taylor, et al., 2012). Similarly, aberrant activation of the WNT signalling pathway leads to development of WNT tumours. Mutations to both the *Adenomatous polyposis coli (APC)* and *beta-catenin (CTNNB1)* genes cause constitutive activation of the WNT signalling pathway, leading to  $\beta$ -catenin accumulating in the nucleus and activating target oncogenes such as *MYC* and *Cyclin D1* (Huse & Holland, 2010; Northcott, Taylor, et al., 2012).

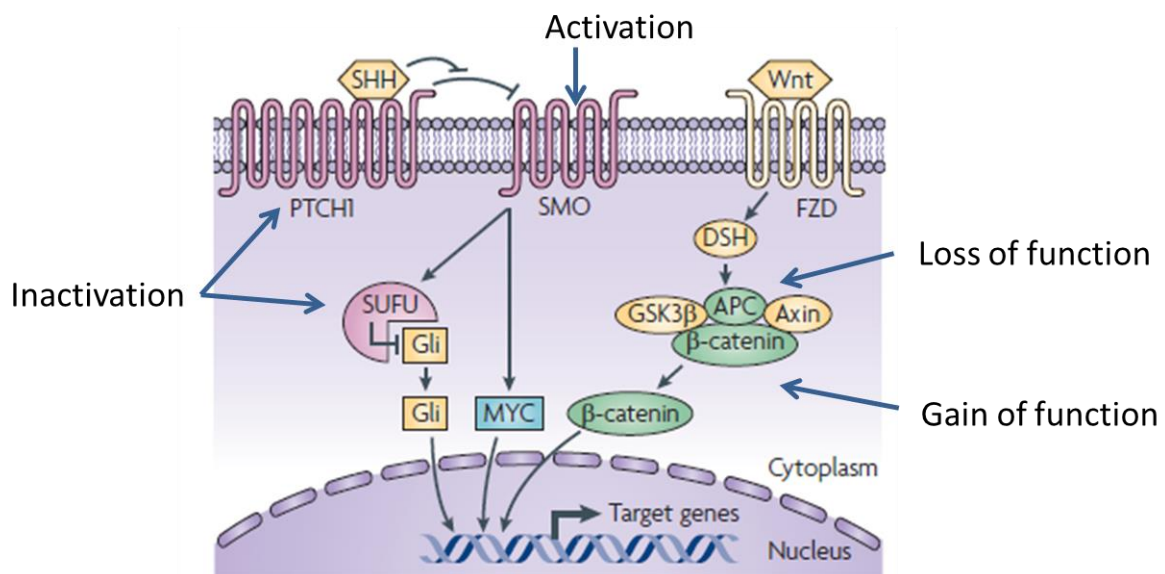


**Figure 1. Sonic Hedgehog (SHH) and Wingless (WNT) signalling pathways**

The SHH and WNT signalling pathways, shown above, have both been implicated in medulloblastoma pathogenesis. Mutations to key pathway intermediates are associated with aberrant over-activation of the respective pathways, and are associated with SHH and WNT medulloblastoma tumours. In the SHH signalling pathway, mutations resulting in the inactivation of PTCH1 and/or SUFU, or activation of SMO cause aberrant SHH signalling. Along the WNT pathway, loss and gain of function mutations to APC and/or CTNNB1 (encoding  $\beta$ -catenin) cause aberrant pathway signalling. Both result in over-expression of target oncogenes. Figure adapted from (Huse & Holland, 2010) .

Murine models have been invaluable in understanding the biology of these medulloblastoma tumours, and from a translational perspective, they are crucial in the development of pre-clinical trials that may lead to the development of much needed targeted therapies. Currently, there are verified mouse models representing SHH, WNT, and Group 3 medulloblastoma (Pöschl et al., 2014), but none for Group 4. There are a number of mouse models with various alterations to the SHH pathway that have been useful in conducting pre-clinical trials for SHH medulloblastoma (Pöschl et al., 2014). Similarly, WNT medulloblastoma, mouse models with mutant CTNNB1 in combination with mutant *TP53*, have been generated to better understand tumour biology, with potential use as models for testing new therapies for WNT medulloblastoma (Gibson et al., 2010; Lau et al., 2012; Pöschl et al., 2014; Remke et al., 2013). Only a single verified murine representation of Group 3 medulloblastoma exists, with aberrant *MYC* expression (Swartling et al., 2010), and unfortunately no mouse model that is representative of Group 4 medulloblastoma currently exists (Pöschl et al., 2014) limiting the development of targeted therapies for one of the most aggressive and metastatic sub-groups. In the future, overexpression of putative Group 4 medulloblastoma oncogenes, such as *DACH1*, may be appropriate for consideration for the development of mouse models representative of Group 4 medulloblastoma.

**Table 1. Summary of key features of the four core medulloblastoma sub-groups**

	Wnt	Shh	Group 3	Group 4
<b>% of cases</b>	10%	30%	25%	35%
<b>5 year survival</b>	>95%	~80%	<50%	~70%
<b>Age group</b>	All ages	0-3 yrs, >6 yrs	Infancy & childhood	Infancy and childhood, usually 3-10yrs
<b>Metastatic dissemination</b>	Rare	Uncommon	Very frequent	Frequent
<b>Key genetic features</b>	Wnt pathway over-activation and mutations  Accumulation of $\beta$ -catenin	Shh pathway over-activation and mutations  MYC amplification  Chromosomal abnormalities	MYC amplification  OTX2 amplification  Chromosomal abnormalities	Mutations to epigenetic modifiers KDM6A and KDM6B, MLL2 and MLL3  Chromosome 17 abnormalities  Loss of an X chromosome in females

Summarised from Min, Lee, Kim, and Park (2013); Northcott, Korshunov, Pfister, and Taylor (2012); Northcott, Schumacher, et al. (2012); Northcott, Taylor, et al. (2012); Schroeder and Gururangan (2014).

## 1.2 Group 3 and Group 4 medulloblastoma

Group 3 and Group 4 medulloblastoma tumours have the highest overall prevalence, poor prognosis, and highest frequency of metastasis (Table 1 and Figure 2). Despite their aggressive nature and frequent occurrence, the molecular pathogenesis of these tumours is not completely understood. There are recurrent abnormalities, including mutations to genes that are associated with chromatin remodelling and overexpression of genes associated with neuronal differentiation in Group 4, and retinal development in Group 3 (Taylor et al., 2012), and frequent amplification of *MYC/MYCN* which is an indicator of poor prognosis (Korshunov et al., 2012; Roussel & Robinson, 2013). There are also characteristic recurrent chromosomal rearrangements, the most common being those that involve chromosome 17, particularly frequent in Group 4 medulloblastoma (Northcott, Schumacher, et al., 2012). While patients with i17q tend to have a poorer outcome, the biology behind this is not known.

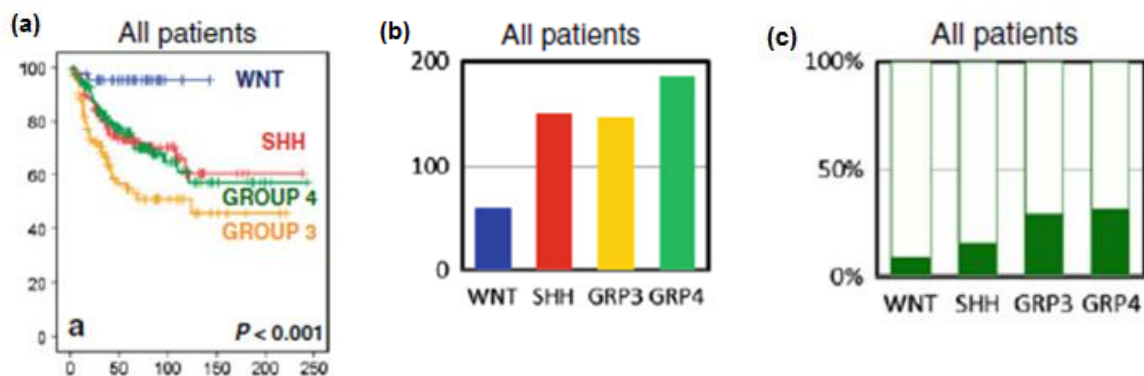


**Figure 2. Distribution of sub-group specific survival, occurrence, and metastasis**

(a.) Patient survival across the four medulloblastoma sub-groups. Group 3 and Group 4 having the worst survival outcome, followed by SHH, and WNT. (b.) Representation of occurrence of each sub-group, Group 4 is most frequently diagnosed, followed by SHH and Group 3, and WNT being the least common. (c.) Presence of metastatic disease in each of the four sub-groups. Metastasis is most common amongst Group 3 and Group 4, and rare in SHH and WNT. (Image adapted from Kool et.al., 2012).

What appears to be most significant in these tumours however, are alterations involving epigenetic modifiers, MLL2 and MLL3, as well as KDM6A and KDM6B (Li, K.K-W., Lau,

K.M., Ng, H.K., 2013; Parsons et al., 2011; Schroeder & Gururangan, 2014). The consistent recurrent alterations to epigenetic modifiers are likely to have a critical role in Group 3 and Group 4 medulloblastoma pathogenesis. Additionally, a change in expression of a number of genes in medulloblastoma has been associated with changes in methylation patterns, pointing to potential players in medulloblastoma pathogenesis (Hovestadt et al., 2014).

### **1.3 Potential mechanisms involved in Group 3 and Group 4 medulloblastoma pathogenesis**

The low frequency of recurrent mutations to common cancer-associated genes suggests an additional level of complexity in medulloblastoma tumours, potentially involving epigenetic regulatory mechanisms at the DNA, histone, and mRNA level (Dubuc et al., 2013; Lindsey, Anderton, Lusher, & Clifford, 2005; Uziel et al., 2009). It is evident that alterations to chromatin modifier genes are present in all sub-groups (for review see Jones, Northcott, Kool, and Pfister (2013)). Most commonly identified across all sub-groups were mutations to the methyltransferase gene MLL2, producing a truncated and non-functional protein (Parsons et al., 2011). Sub-group specific alterations to other epigenetic modifying genes are also observed, with both Group 3 and Group 4 showing characteristic alterations that generally result in elevated methylation of Histone 3, lysine 27 (H3K27me3). In Group 4, there are also recurrent mutations to the Histone 3 Lysine 27 (H3K27) histone demethylase, KDM6A, which produce a non-functional protein (Dubuc et al., 2013). In Group 3 WNT tumours, SMARCA4 mutations are common, while in SHH sub-group tumours, alterations to the nuclear receptor co-repressor (N-CoR) complex are prevalent (Jones et al., 2013).

Such recurrent changes inevitably impact on the epigenetic regulation of downstream tumour suppressor and oncogenes. In support of this, a recent analysis by Hovestadt et al. (2014) assessed DNA methylation and gene expression levels across all medulloblastoma sub-groups, and demonstrated that level of expression was correlated to methylation status of numerous genes (Hovestadt et al., 2014). This insight provides a better understanding of the importance of epigenetic alterations in medulloblastoma tumourigenesis.

Additional mechanisms of genetic regulation at a post-transcriptional level have an equally important role in regulation of gene expression. microRNAs are of note here, and will be discussed below in section 3.0.

## **2.0 DACHSHUND HOMOLOG 1**

The *Dachshund Homolog 1 (DACH1)* gene is a homolog of the *Drosophila dac* gene, a regulator of cell fate determination in *Drosophila* eye, limb, and brain development. *Dac* is an important component of the *Drosophila* retinal determination gene network (RDGN) for specifying of retinal cell fate and promoting photoreceptor differentiation and programming retinal progenitor cells (Atkins et al., 2013; Davis, Mardon, et al., 2001; Mardon, Solomon, & Rubin, 1994). Mammalian homologues of *dac* -DACH1 and DACH2- show similar function in the regulation of cell fate determination and cell proliferation, and are both important in embryonic development, with some redundancy in their role (Davis, Shen, Sandler, Heanue, & Mardon, 2001). In mice DACH1 is critical for post-natal survival and development and lethal when not expressed, with homozygous DACH1 knockout mice not surviving past postnatal day one (Davis, Mardon, et al., 2001).

In humans, the DACH1 gene, 429,233 bases long, is located on chromosome 13q22, and has three alternative transcripts. The main DACH1 isoform is translated into a 97kDa protein (Davis, Shen, Heanue, & Mardon, 1999). There are two functional domains, located at the C-terminus (DachBox-C) and N-terminus (DachBox-N) (Tavsanli et al., 2004), and these binding domains enable DACH1 to modulate transcription by direct DNA binding or interaction with other proteins, regulating cell function in a context-dependent manner (Tavsanli et al., 2004; Zhou et al., 2010).

The context in which DACH1 is expressed varies, but the major functions include regulation of cell proliferation and growth, and regulation of cell migration. Evidently, aberrant expression of DACH1 has implications in the pathogenesis in several cancer types.

### **2.1 DACH 1 as a Tumour Suppressor**

Reduced expression of DACH1 is a common feature in many cancers, and is accompanied by changes in cell function including increased cell proliferation, migration, and tumour progression. The tumour suppressive behaviour of DACH1 is well described in breast cancer, where it also has clinical relevance, with reduced expression of DACH1 associated with tumour progression and metastasis, and poor survival (Desmond et al., 2014; K. Wu et al.,

2006). Additional studies have led to the identification of other cancers with reduced DACH1 expression, including prostate cancer, lung cancer, and gastrointestinal cancers, as well as others.

In breast cancer, DACH1 is linked to the regulation of cell cycling and cell proliferation by antagonizing transcription factors such as c-Jun and FOXM1 and blocking DNA synthesis and target gene expression associated with cell cycling (K. Wu et al., 2007; Zhou et al., 2010). Additionally, DACH1 demonstrates anti-migratory function via inhibition of IL-8 to repress pro-metastatic oncogenes *MYC*, *RAS*, and *ErbB2* in breast cancer (Kongming. Wu et al., 2008), and blocking YB-1 transcription factor to maintain E-cadherin expression and epithelial phenotype (Wu et al., 2014)

Several studies have confirmed that restoring DACH1 expression results in reduced DNA synthesis, cell proliferation, contact-independent growth, cell growth, and reduced tumour size in cell lines and in mice (Wu et al., 2014 Wu et al., 2008, Wu et al., 2014., Yan et al., 2014) . In addition, altered TGF- $\beta$  signalling is associated with loss of DACH1, showing increased expression in early stages of cancer, and reduced expression in advanced invasive cancers (Wu et al., 2014, Yan et al., 2014). .

DACH1 is also involved in regulating epithelial-mesenchymal transition (EMT), and is implicated in metastatic progression. Briefly, DACH1 repression of YB-1 inhibits induction of transcription factors such as ‘Snail’ which regulate expression of epithelial marker E-cadherin as well as other targets (Wu, K., et al., 2014). Ultimately, repression of Snail via YB-1 enables expression of E-cadherin and maintains a non-invasive epithelial phenotype. DACH1 association with EMT also extends to the inhibition of TGF- $\beta$  signalling, which is lost in later stage cancers and is associated with EMT and gaining invasiveness (Yan et al., 2014). These proposed mechanisms of DACH1 and EMT are outlined in Figure 3.

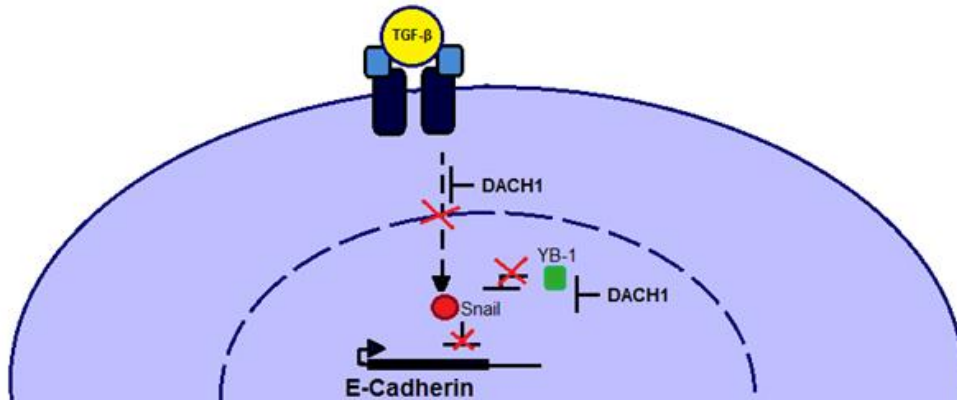


**Figure 3. Mechanisms of DACH1-mediated inhibition of Epithelial-Mesenchymal Transition (EMT):** Expression of DACH1 inhibits TGF- $\beta$  signalling in later-stage cancers, and also represses the Y-Box1 transcription factor. These block the expression of transcription factor Snail, an inhibitor of E-cadherin, enabling the cell to maintain expression of the epithelial marker E-cadherin.

## 2.2 DACH1 as an oncogene

Consistent with the pleiotropic properties of DACH1, there are cancers that show elevated DACH1 expression, often associated with advanced cancers with poor prognosis. Higher levels of DACH1 are associated with cancer progression in ovarian cancer, pre-invasive colorectal tumours (colorectal adenomas) and colorectal carcinomas, and leukaemia's (Lee et al., 2012; Liang et al., 2012; Vonlanthen et al., 2014).

Various studies suggest that the level of DACH1 expression is associated with tumour stage and progression, with clinical relevance for predicting patient prognosis. In ovarian cancer, DACH1 is associated with reduced TGF- $\beta$  expression, and increased cell proliferation (Sunde et al., 2006), and also shows relevance to tumour stage, with increasing levels present as tumours progress towards metastasis (Liang et al., 2012). Similarly, in colorectal tumours, DACH1 is predicted to have an important role in tumourigenesis. Analysis of transcription factor expression in colorectal adenomas and colorectal cancer indicated that DACH1 may be important in tumour progression, with increased DACH1 in pre-invasive tumours that is associated with highly proliferative cells (Liang Wu et al., 2014). Although the mechanisms underlying DACH1's role as an oncogene have not been fully explored, in hematopoietic cells at least, elevated DACH1 has been linked to abnormalities in cell cycling and cell differentiation (Lee et al., 2012).

### **2.3 DACH1 expression in medulloblastoma**

Gene expression profiling of a series of human medulloblastoma revealed that DACH1 shows elevated expression across all medulloblastoma sub-groups compared to normal cerebellum. DACH1 is most highly expressed in Group 4 (Figure 4.). Additionally, a recent study investigated the level of gene expression across all medulloblastoma sub-groups, DACH1 included, according to methylation status. This showed that increased expression of DACH1 is associated with reduced methylation in medulloblastoma, and was highly associated with Group 4 medulloblastoma (Hovestadt et al., 2014). Currently, the precise mechanisms driving the overexpression of DACH1 in Group 4 medulloblastoma have not been investigated.

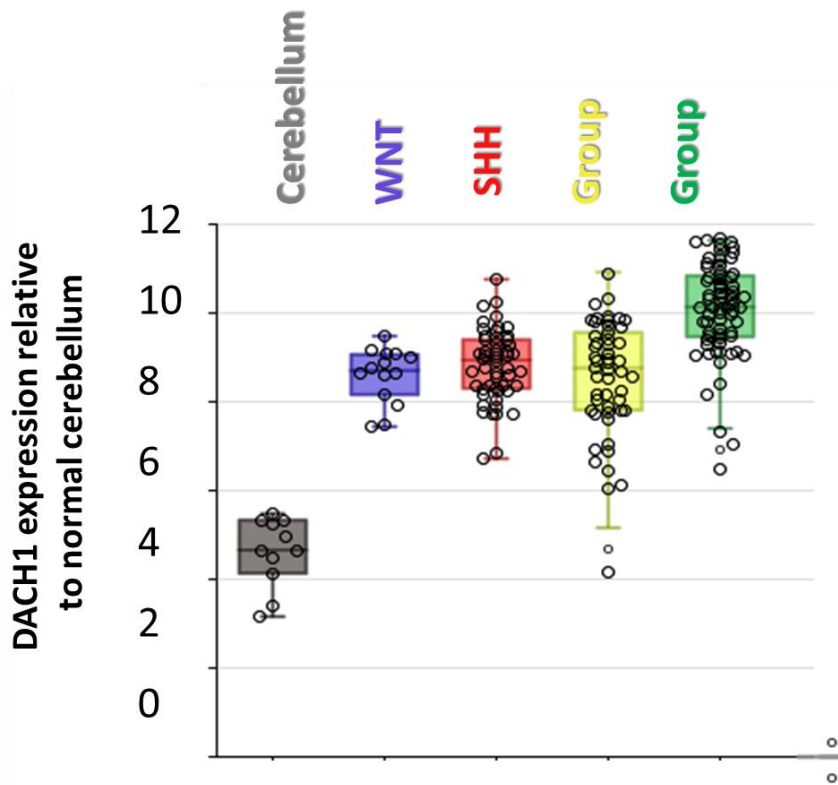


**Figure 4. DACH1 expression across all sub-groups**

DACH1 expression is elevated across all four medulloblastoma sub-groups compared to normal cerebellum, highly expressed in Group 4 medulloblastoma (Adapted from Mark Remke, University of Toronto, Pers Comm).

## 2.4 Regulation of DACH1 expression

The level of DACH1 expression appears to be an important factor in cancer progression; however the mechanisms involved have not been fully described for all cancers. Epigenetic mechanisms have been proposed and are generally the most frequent abnormalities that account for aberrant DACH1 expression. Promoter methylation is seen amongst several cancers that show reduced DACH1 expression (Liang Wu et al., 2014; Yan et al., 2013; Yan et al., 2014; H. Zhu et al., 2013), and indeed in medulloblastoma, hypomethylation of the *DACH1* gene is associated with overexpression (Hovestadt et al., 2014). Epigenetic alterations directly affecting the *DACH1* gene, combined with frequent alterations to epigenetic modifiers in Group 3 and Group 4 medulloblastoma that may also impact DACH1 expression is consistent with a major role for epigenetic modulation of DACH1 expression in medulloblastoma pathogenesis. One important epigenetic mechanism that may be involved in modifying DACH1 expression is post-transcriptional regulation by microRNAs.

### 3.0 MicroRNA

MicroRNAs (miRNAs) belong to a class of small non-coding RNA molecules approximately 22 nucleotides in length, and are recognised as important regulators of cell function. Their biogenesis is outlined in Figure 5. Briefly, in the nucleus miRNAs are transcribed from the respective miRNA gene by RNA polymerase II, into long primary microRNAs (pri-miRs). Cleavage by the ribonucleases Drosha and Pasha (DGCR8) generates a hairpin pre-cursor miRNAs (pre-miR) that are then exported from the nucleus. The pre-miRs are then further processed by the ribonuclease Dicer and transactivation-responsive RNA-binding protein (TRBP) into two short single stranded miRNAs- leading and passenger, the latter of which is considered non-functional. Once associated with the RNA-induced silencing complex, the ‘leading’ strand guides this complex along the target mRNA where binding will initiate target degradation or repression (see reviews Fabbri, Croce, & Calin, 2008; Finnegan & Pasquinelli, 2013).

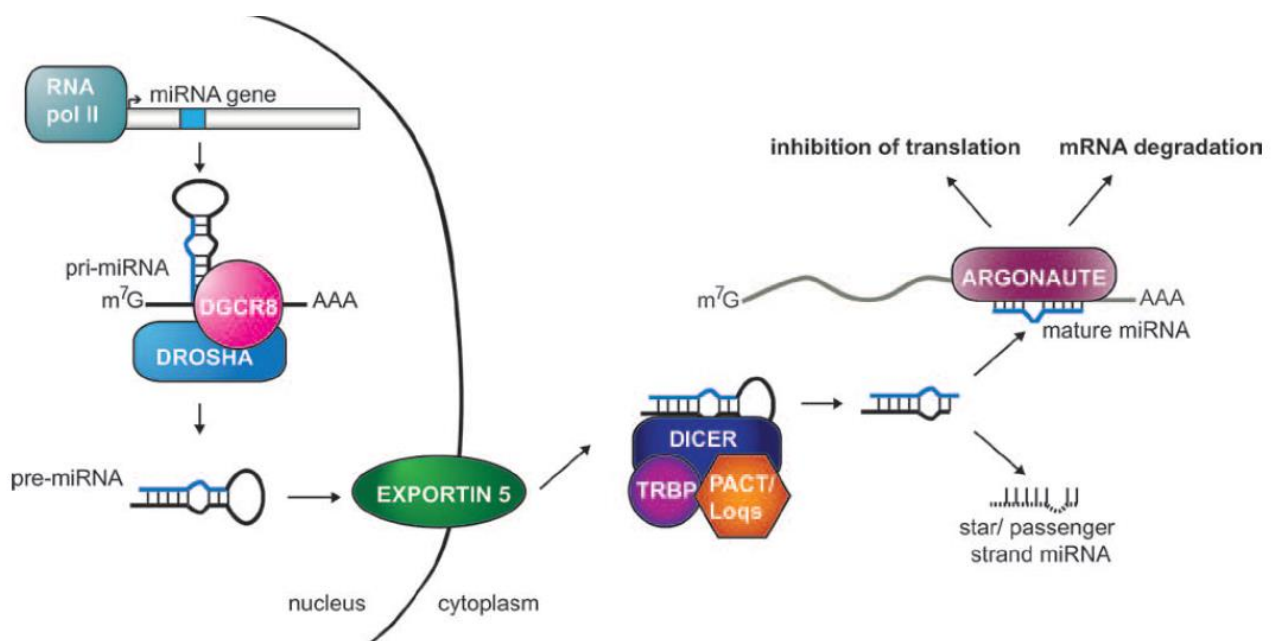


**Figure 5. The typical miRNA biogenesis pathway**

miRNAs are transcribed by RNA polymerase II, and processed in the nucleus by various ribonucleases, into premature miRNA (pre-miR). The pre-miR is transported from the nucleus and undergoes further modification to generate two single stranded

RNAs, one of which will interact with the RISC complex and initiate repression of translation of target degradation (Finnegan & Pasquinelli, 2013).

### **3.1 microRNAs and cancer**

miRNAs are capable of binding with high specificity to target mRNAs to regulate post-transcriptional gene expression. Specifically, miRNAs bind to their target via Watson-Crick base-pairing, recognising a seed sequence within the 3' untranslated region (UTR) of a target mRNA (Doench & Sharp, 2004). Such binding targets mRNA for degradation or by blocking translation. This mechanism of post-transcriptional modification has provided new insight into an additional level at which gene expression can be regulated, and has demonstrated their importance in regulating normal cellular processes, as well as their role in tumourigenesis. miRNAs have the capacity to function in a similar manner to tumour suppressors and oncogenes when aberrantly expressed and are collectively referred to as oncomirs (Cho, 2007; Esquela-Kerscher & Slack, 2006). A comparison between normal and abnormal miRNA expression is shown below in Figure 6.

So far, a number of microRNAs have been identified as key determinants in cancer, many of which share a common role in different cancer types. For example, the over-expression of miRNAs such as miR-155 and the miR-19~72 cluster repress tumour suppressors leading to overexpression of oncogenes such as MYC. Others, such as miR-21 are functionally involved in cancer progression and are also markers of poor prognosis (Cho, 2007; Huang et al., 2013; S. Zhu et al., 2008). A more comprehensive understanding of the functional importance of such miRNAs in cancer, will be invaluable for better understanding the role of these molecules not only in the context of disease, but also in normal cellular physiology (Kong, Ferland-McCollough, Jackson, & Bushell, 2012).

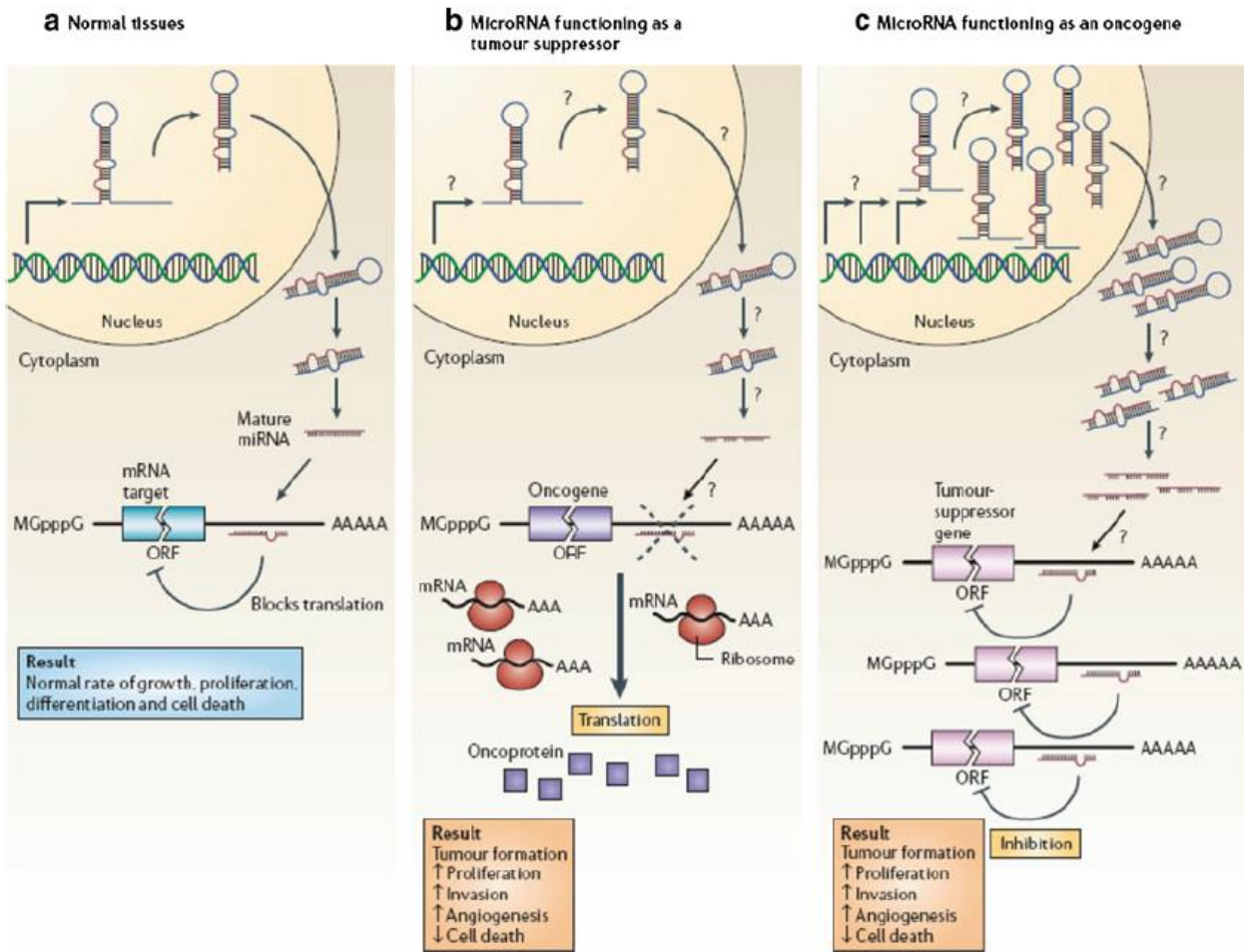


**Figure 6. The normal and abnormal behaviour of microRNAs**

(a.) The normal function of microRNA, regulating cellular processes by blocking translation of specific target genes. (b.) Tumour suppressive role of miRNA is lost due to deregulated miR expression resulting in the aberrant over-expression of oncogenes. (c.) A gain in oncogenic microRNA expression results in abnormal degradation of the tumour suppressive targets. (Image taken from Huang et al., 2013) (DeSouza et al., 2014) (DeSouza et al., 2014) (DeSouza et al., 2014) (DeSouza et al., 2014)

### 3.2 microRNA and medulloblastoma

The first study miRNA study profiling medulloblastoma tumours was conducted by Ferretti et al. (2009), and identified a number of over- and under-expressed microRNAs in medulloblastoma tumours and cell lines, as compared to normal cerebellum. Many microRNAs demonstrated potential tumour suppressive activity, including miR-9 and

miR125a. When transfected into the medulloblastoma cell line D283, both induced changes in cell proliferation and increased cell apoptosis (Ferretti et al., 2009).

Continued efforts have identified numerous other candidate miRNAs in medulloblastoma pathogenesis, and have focused on determining the functional significance of these miRNAs, as well as identifying sub-group specific miRNAs that may provide prognostic markers. miR-124 is a tumour suppressive miRNA in medulloblastoma, and loss of expression is associated with uncontrolled cell proliferation as a result of increased Cyclin-Dependent Kinase 6 (CDK6) expression. Evidently, increased miR-124 is capable of silencing CDK6 expression, and has the potential as a therapeutic to block tumour growth (Silber et al., 2013). Similarly miR-22 is also down-regulated in medulloblastoma. Re-introducing miR-22 by transfection increased apoptosis in-vitro, and also in-vivo, as well as reducing tumour size in xenograft models, which was hypothesised to be, at least in part, due to targeting of the 3'-phosphoadenosine 5'-phosphosulfate transporter 1 (PPAST1) gene (Xu et al., 2014).

Additionally, over-expressed miRNAs in medulloblastoma have also been identified. A study by Genovesi, Carter, Gottardo, Giles, and Dallas (2011) compared miRNA profiles between medulloblastoma and humans neural stem cells, a predicted cell of origin in Group 3 and Group 4 medulloblastoma, and reported frequent up-regulation of miRNAs that are involved in regulation of neuronal migration and signalling. Several others have an apparent role in metastasis. For example, the miR-183~96~182 cluster is associated with the more aggressive medulloblastoma tumours, with miR-182 in particular, being capable of inducing an invasive/metastatic behaviour in vitro, and is associated with tumour invasion to surrounding tissue in mouse models over-expressing miR-182 (Bai et al., 2012). A further study noted changes in gene expression, specifically an up-regulation of transcription factors involved in the regulation and promotion of epithelial-mesenchymal transition (EMT). This suggests that the miR183~92~182 cluster may confer changes in invasiveness via epithelial-mesenchymal transition (EMT) (Weeraratne et al., 2012). The EMT pathway is one which has been well described for its role in tumour metastasis, and is discussed below.

### **3.3 Epithelial-mesenchymal transition (EMT)**

The metastatic process refers to a sequence of events that occur as tumour cells gain the ability to invade surrounding tissue and disseminate within the body. These changes in cancer cell phenotype are the result of changes in gene expression leading to loss in cell adhesion, gaining mobility, and gaining the capacity to disseminate (Nguyen & Massagué, 2007). EMT involves a complex network of signalling molecules, transcription factors, and microRNAs, which regulate the transition of epithelial cells towards a mesenchymal phenotype, and the development of features that favour metastatic dissemination. Thus aberrant activation of EMT has been implicated as an early process in metastatic cancer (D'Amato, Howe, & Richer, 2013).

#### ***3.3.1 microRNAs, EMT, and metastasis***

There is abundant evidence for the crucial role of miRNAs in all stages of cancer pathogenesis. In metastasis, the important regulatory role of miRNA, and the impact of deregulated microRNA expression on metastatic progression, has been well documented. The importance of microRNAs in the regulation of epithelial-mesenchymal transition and metastasis will be the focus here.

EMT is a dynamically regulated process and there are multiple levels through which expression can be regulated. microRNAs are key, and their loss or gain of expression has implications on EMT and metastasis. Figure 7 highlights some of the important miRNA regulators in EMT. To elaborate on some of these; expression of both miR-21 and miR-9 promote metastasis, with miR-21 promoting invasiveness and metastasis in many cancers (Cottonham, Kaneko, & Xu, 2010; D'Amato et al., 2013; Huang et al., 2013). Meanwhile miR-9 directly controls E-cadherin expression as a pleiotropic pro-metastatic oncogene (Ma et al., 2010; Zhang & Ma, 2012). Conversely, there are miRNAs whose expression can suppress EMT, such as the miR-200 family whose role in metastasis will be described below.

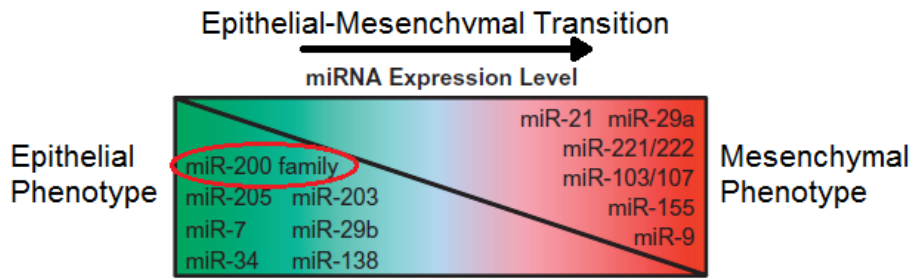


**Figure 7. miRNA expression in EMT**

Several microRNAs are important in maintaining EMT, whose expression may be oncogenic and maintain a mesenchymal phenotype, or tumour suppressive whose expression maintains epithelial phenotype. Expression of these miRNAs determines whether the cell maintains an epithelial or a mesenchymal phenotype. (Image adapted from D’Amato et al., 2013).

### 3.3.2 The miR-200 family and miR-200b in EMT

The miR-200 family consists of five members; miR-200a, miR-200b, miR-200c, miR-429, and miR-141, belonging to two clusters on chromosome 1p36 (miR-200b/c and miR-429), and 12p13 (miR-200a and miR-141). They share highly conserved seed sequences which differ by only a single nucleotide (Feng, Wang, Fillmore, & Xi, 2014) (Figure 8).



**Figure 8. The miR-200 family members have two conserved seed sequences**

Two clusters of the miR-200 family; miR-200b/c/429 and miR-200a/141, share seed-sequences differing by a single nucleotide. (Sequences obtained from miRBase, 2014).

In cancer, miR-200 functions as an important tumour suppressor. Loss of expression of the miR-200 family is evident in many cancers, and is associated with poor survival, increased cell proliferation, and in particular, an invasive/metastatic phenotype (Hailin et al., 2013; Men, Liang, & Chen, 2014). Members of the miR-200 family are involved in the regulation of EMT and maintaining an epithelial phenotype, with loss of expression most commonly associated with a metastatic phenotype (Feng et al., 2014; Park, Gaur, Lengyel, & Peter, 2008). Reduced expression of miR-200b may be a consequence of altered epigenetic mechanisms causing promoter hypermethylation affecting the miR-200b cluster which is consistent with reduced expression in medulloblastoma.

Members of the miR-200 family specifically regulate the transcription factors (ZEB1 and Zeb2), and form a negative regulatory feedback loop to regulate expression of the epithelial cell adhesion molecule E-cadherin (Ding, 2014). To elaborate, ZEBs are negative regulators of E-cadherin, and expression results in loss of the epithelial marker E-cadherin, which is evident during EMT (Barry et al., 2008; Korpala, Lee, Hu, & Kang, 2008). miR-200 family members are inhibitors of ZEBs, and their expression maintains epithelial phenotype. Likewise ZEBs negatively regulate miR-200 and maintain mesenchymal cell phenotype. A simplified overview of miR-200 role in EMT is presented below in Figure 9.

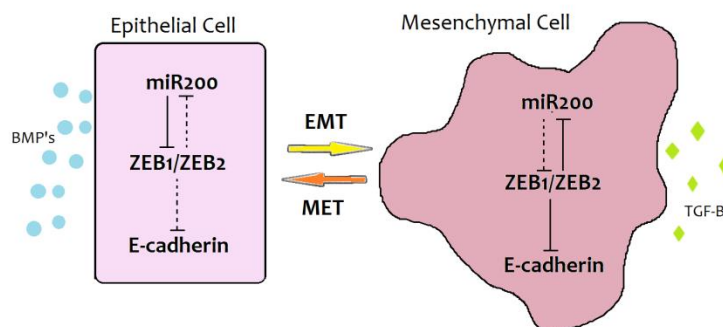


**Figure 9. Simplified overview of the regulatory role of miR-200 in EMT**

In epithelial cells; ZEB1 and ZEB2 are EMT-inducing transcription factors regulated by miR-200, and repress the expression of E-cadherin. In epithelial cells, the miR-200 family inhibits the expression of ZEB1 and ZEB2. Ultimately this enables expression of E-cadherin and maintenance of the epithelial cell phenotype.

Loss of miR-200 expression is predicted to be a vital step in the metastatic process, and certainly this phenomenon may be important in highly metastatic cancers such as medulloblastoma. Previously, the loss of miR-200 expression has been reported in metastatic prostate cancer, breast cancer, colorectal cancer, lung cancer, gastric cancer, and others (Feng et al., 2014). Different members of the miR-200 family alone, have been identified as potential prognostic markers with a proposed prognostic role in glioma and breast cancer (Men et al., 2014; Ye et al., 2014), and are able to regulate invasiveness individually. For example, over-expression of miR-200b in prostate and gastric cancer results in reduced invasiveness that is predicted to be due to reversal of EMT (Hailin et al., 2013; Williams, Veliceasa, Vinokour, & Volpert, 2013a, 2013b). Although miR-200 expression has not been investigated in medulloblastoma pathogenesis, given the role of deregulated expression of the miR-200 family in promoting metastasis in various contexts suggests that loss of miR-200b function may contribute to medulloblastoma pathogenesis and metastasis.

Medulloblastoma tumours have a high propensity to metastasise, with around 30% of tumours showing dissemination at diagnosis, linked to poor prognosis (Gerber et al., 2014). Therefore, effectively targeting metastatic medulloblastoma cells at a molecular level may prove to be a valuable therapeutic. miRNA expression profiling in medulloblastoma cell lines within this laboratory has revealed down-regulation of miR-200b in medulloblastoma cell lines that are representative of the aggressive Group 3 sub-group, consistent with a potential role in metastatic medulloblastoma. Additionally, *in-silico* analysis of the DACH1 3'-UTR (TargetScan Human Release 6.2) revealed a potential binding site for nine miRNA/clusters (Figure 10a). miR-200b was one of the miRs identified as having a high probability of binding to the DACH1 3'UTR at position 971-978 in the 2689 nucleotide (nt) 3'UTR (Figure 10b).

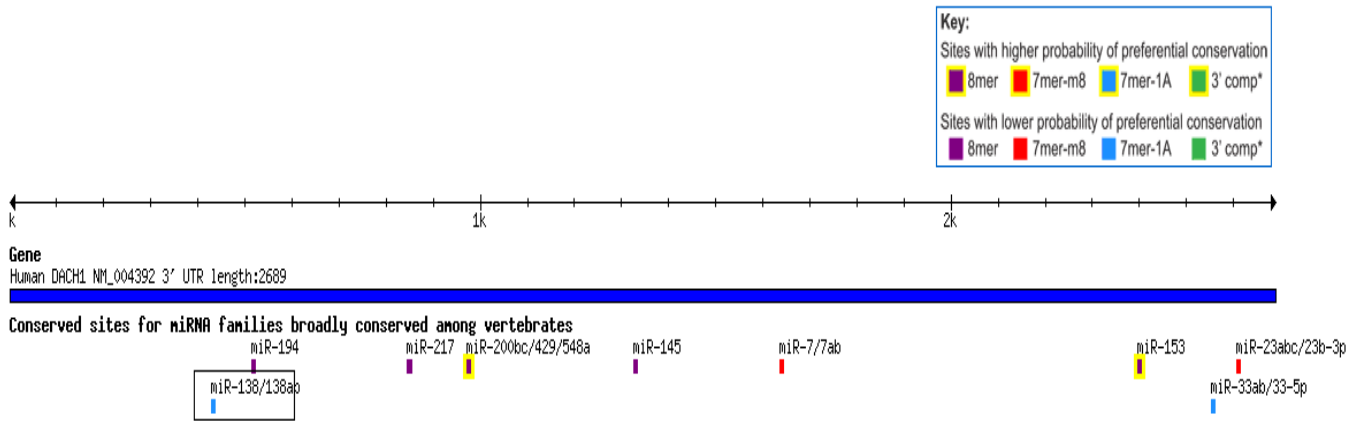


**Figure 10a. TargetScan putative miRNA binding sites**

TargetScan identifies nine clusters of miRNAs with potential binding sites in the DACH1 3'UTR. Two have 8-mer binding sites with high probability of binding (hsa-miR200b/c/429 and hsa-miR-153), while the remaining have a low probability 7-mer and 8-mer potential binding sites

	predicted consequential pairing of target region (top) and miRNA (bottom)	seed match	site-type contribution	3' pairing contribution	local AU contribution	position contribution	TA contribution	SPS contribution	context+ score	context+ score percentile	conserved branch length	P <sub>CT</sub>
Position 971-978 of DACH1 3' UTR	5' ... AUUUGUCUGGAGUCACAGUAUUA... 3' UGCCCCAAUUGGUCUGUCAUAAU	8mer	-0.247	0.024	-0.028	0.131	0.023	0.096	> -0.03	37	2.002	0.87
hsa-miR-429	3' UGCCCCAAUUGGUCUGUCAUAAU											
Position 971-978 of DACH1 3' UTR	5' ... AUUUGUCUGGAGUCACAGUAUUA... 3' AGUAGUAAUGGUCGCAUAAU	8mer	-0.247	0.024	-0.028	0.131	0.023	0.096	> -0.03	36	2.002	0.87
hsa-miR-200b	3' AGUAGUAAUGGUCGCAUAAU											
Position 971-978 of DACH1 3' UTR	5' ... AUUUGUCUGGAGUCACAGUAUUA... 3' AGGUAGUAAUGGCGUCAUAAU	8mer	-0.247	0.024	-0.028	0.131	0.023	0.096	> -0.03	36	2.002	0.87
hsa-miR-200c	3' AGGUAGUAAUGGCGUCAUAAU											

**Figure 10b. miR-200 family target sequence within the DACH1 3'UTR**

Members of the miR-200 family cluster miR-200b/c/429 have an 8-mer sequence within the DACH1 3'UTR, with a high probability of binding. miR-200b is highlighted.

#### **4.0 SUMMARY**

The exact pathogenic mechanisms driving elevated DACH1 expression are unclear, but current evidence suggests elevated DACH1 plays an important role in tumour growth, progression, and metastasis. DACH1 is a putative oncogene in medulloblastoma, over-expressed in all four sub-groups of medulloblastoma, most noticeably in Group 4 medulloblastoma. Its previous links with metastasis supports the potential role of DACH1 in progression of metastatic Group 4 medulloblastoma. In addition, it is possible that the over-expression of DACH1 is a consequence of aberrant epigenetic regulation, such as loss of miRNA regulation. In medulloblastoma, miR-200b is down regulated, and has putative binding site within the DACH1 3'UTR, suggesting a potential for miR-200b to be involved in regulation of DACH1 expression.

## 4.1 AIMS

We hypothesise that miR-200b regulates DACH1 and that this relationship is significant in aggressive Group 3 and Group 4 medulloblastoma pathogenesis. Our aims therefore are:

1. To confirm an inverse correlation between DACH1 and miR-200b in medulloblastoma cells using quantitative reverse transcription polymerase chain reaction to assess miR-200b and DACH1 mRNA.
2. To generate reporter cell lines via stable transduction of a DACH1-3'UTR-lenti-reporter-GFP virus, and assess the effect of miRNA on reporter protein expression.
3. Transiently transfect cells with miR-200b, and assess for any changes in DACH1 mRNA or protein expression, using qRT-PCR and Western Blot.

## 5.0 METHODS

### 5.1 Cell culture:

Medulloblastoma cell lines DAOY, UW228, PER547, D283, D341, and D425 cells were cultured at 37°C, in 5% CO<sub>2</sub>. These cells were maintained as follows:

**Table 2 Cell line details and culture conditions**

	<b>Cell line details</b>	<b>Culture conditions</b>
<b>DAOY</b>	Representative of Sonic Hedgehog (SHH) medulloblastoma (Jacobsen, 1985)	Adherent cells, grown as a single monolayer DMEM (Gibco®, Invitrogen™, LifeTechnologies™, Carlsbad, Canada) + 10%FCS + 1% Glutamax (Gibco®), harvested with 0.05% dissociation reagent (TrypsinEDTA) (Gibco®) and subcultured at 1:20 when cells reached 90% confluence
<b>UW228</b>	Representative of Sonic Hedgehog (SHH) medulloblastoma (Keles, 1991)	Adherent cells, grown as a single monolayer MEM (Gibco®) + 10% FCS + 1% Glutamax (Gibco®), harvested with 0.05% trypsin, subcultured 1:20 when cells reached 90% confluence
<b>PER547</b>	Representative of Group 3 medulloblastoma (Holthouse et al., 2008)	Suspension cells (1:6) RPMI (Gibco) + 20% FCS + Glutamax (Gibco®) + non-essential amino acids (NEAA) 100x (Gibco®) + Sodium pyruvate (NaP) 100nM (Gibco®)+ 1.8mL 2-mercaptoethanol (2-ME) (Sigma Aldrich®, St. Louis, Missouri), cells were subcultured 1:6 when 80-90% confluent
<b>D283</b>	Representative of Group 3	Semi-adherent cells (1:3)

	medulloblastoma (Friedman, 1985)	MEM (Gibco®) + 20% FCS + 1% Glutamax (Gibco®), cells were subcultured when 80-90% confluent
<b>D341</b>	Representative of Group 3 medulloblastoma (Friedman, 1988)	Suspension cells. (1:3) MEM (Gibco®) + 20% FCS + 1% Glutamax (Gibco®), cells were subcultured when 80-90% confluent
<b>D425</b>	Representative of Group 3 medulloblastoma (He, 1991)	Semi-adherent cells. 1:5 Modified MEM (Gibco®) + 10% FCS + 1M HEPES (Gibco®), cells subcultured when 80-90% confluent

Adherent cells were harvested by removing medium then briefly washed in 5-10mL of DPBS (Gibco®). 5-10mL of 0.05% dissociation reagent. Cells were incubated for 5 minutes at 37°C and then mechanically dissociated from plate. Cells were collected in a 5mL tube, then diluted 1:20 and re-plated in a T25 flask (nunc) with 5mL of growth medium, or a T75 with 10mL of growth medium. Note that cells were re-plated while suspended in trypsin.

Semi-adherent/suspension cells were harvested by mechanical pipetting to dissociated cells and collected in a 50mL Falcon tube. Cells were split in a 1:3-1:6 ratio depending on growth rate. Cells were plated in 1mL of medium in a 24 well plate (nunc).

### ***5.1.1 Countess: cell number and viability***

10µL of harvested cells were aliquoted with 10µL of 0.2% Trypan Blue (TB) (Sigma Aldrich®) (1:1 ratio). 10µL was then counted using the Countess™ automated cell counter (Invitrogen™, Life Technologies™).

## 5.2 Protein Extraction

1.0-4.0x10<sup>6</sup> cells were pelleted in using a HERAEUS Multifuge 35R+ (ThermoScientific, Waltham, Massachusetts) at 900rpm for 5 minutes, and resuspended in PBS buffer (-Mg<sup>2+</sup> and -Ca<sup>2+</sup>, Gibco®), then re-pelleted. Cells were lysed in 70µL radioimmunoprecipitation assay (RIPA) buffer (150mM NaCl, 50mM Tris HCL pH8, 1% NP-40, 0.5% Sodium deoxycholate, 0.1% SDS with complete mini EDTA free and phos-stop inhibitors (Roche, Switzerland). The Lysate was then centrifuged 13,000rpm for 20minutes at 4°C (HERAEUS Fresco17, ThermoScientific) to pellet debris, and protein was quantified using a Direct Detect™ Spectrometer (Merck Millipore, Billerica, Massachusetts).

## 5.3 SDS polyacrylamide gel electrophoresis (SDS-PAGE) and immunoblotting

Total protein (30µg), was adjusted to 20µl with the addition of 2µl 10x reducing agent and 5µl 4x loading buffer. Samples were denatured at 70°C and run on 3-8% Tris Acetate gel (NuPAGE®, Life Technologies™) at 145V for 65 minutes at room temperature, in Tris Acetate running buffer. Precision plus protein™ Dual Colour standards (BioRad, Hercules, California).

Protein was transferred to BioRad 0.2µM nitrocellulose membrane (1620112) in 1x NuPAGE® (Life Technologies™) transfer buffer, 20% methanol, at 30V for 120 minutes, at 4°C. Following transfer, membranes were stained with Ponceau S (0.1% Ponceau S, 7% glacial acetic acid) to monitor efficiency of protein transfer. Membranes were subsequently blocked for 1 hour at room temperature in blocking solution (5% skim milk powder in 1xTBS/0.1% Tween-20), and washed 3x5minutes in 1xTBS/0.1% Tween-20.

Primary antibody; rabbit anti-human DACH1 polyclonal antibody (10914-1-AP, raised against amino acid residues 350aa in the C-terminus) (Proteintech™, Chicago), was diluted 1:1000 with 5µL in 5mL antibody diluent buffer (1% Skim milk powder, 1% BSA in 1xTBS/0.1% Tween-20) and incubated overnight (O/N) at 4°C on a shaker. Membrane was washed 3x5min in 1xTBS/0.1% Tween-20.

The membrane was incubated with ECL Rabbit IgG, HRP-linked F(ab)<sub>2</sub> secondary antibody (NA9340V) (GE healthcare, Wisconsin), diluted 1:5000 with 1µL antibody in 5mL of antibody diluent, for 1 hour at room temperature.

SuperSignal West Dura Extended Duration Substrate (ThermoFisher Scientific) was used for signal detection, and immunoblots were visualised using ChemiDoc MP Imaging System (Bio-Rad).

β-actin was used as a loading control; Primary antibody monoclonal anti β-actin antibody, mouse (A1978) (Sigma Aldrich®), and ECL Mouse IgG, HRP-linked F(ab)<sub>2</sub> secondary antibody (NA9310V) (GE healthcare), diluted 1:5000, incubated at room temperature for 1 hour each and developed as described above.

#### **5.4 Extraction of total RNA**

In most cases, total RNA (including mRNA and miRNA) was extracted from cell lines using a miRNeasy kit (QIAGEN, Cat No: 217004) following the recommended protocol for isolation of miRNA-enriched total RNA.

Briefly, cells were harvested as described and pelleted by centrifugation (HERACUS Multifuge35R, ThermoFisher) in a 25mL Falcon tube (BD Falcon, USA) at 900rpm for 5 minutes. Cells were washed once\* in 1mL DPBS (Gibco®) (\*Adherent cells were washed twice) and counted using the Countess automated cell counter (Invitrogen™, Life Technologies™) as described. DPBS (Gibco®) was removed and cells were resuspended in 350-700µL of QIAzol lysis reagent (QIAGEN). To mix, the suspension was vortexed and incubated at room temperature for 5minutes. Lysate was then extracted by adding 70-140µL of Phenol-chloroform and incubating at room temperature for 2 minutes, then centrifuged 12000rpm/15 minutes (HERAEUS Fresco17, ThermoScientific). The upper phase was removed (approximately 100µL) and added with 1.5 volumes of 100% ethanol. Washes were performed with buffer RWT and buffer RPE and purified RNA was eluted in RNase-free water and quantified using nano drop spectrophotometer (ThermoScientific). RNA with a

260/280 ratio of >1.8 was considered to be of suitable quality and RNA integrity was further assessed by electrophoresis on a 1.5% agarose gel.

## 5.5 TaqMan® Gene expression assays

Two-step quantitative reverse transcription polymerase chain reaction (qRT-PCR) was performed to assess DACH1 mRNA expression in DAOY, UW228, PER-547, D283, D341, and D425. Gene expression assays were performed as per TaqMan® (Applied Biosystems ABI®, Life Technologies™) recommended protocol, using 200ng of total RNA in a 20µL reaction, and reverse transcribed using SuperScript® VILO™ master mix (Invitrogen™, life technologies™) with random primers.

Reverse transcription reactions were prepared using 4µL SuperScript® VILO™ (Invitrogen™) master mix with SuperScript® III Reverse Transcriptase and a final concentration of 200ng/µL of total RNA. Conditions for RT were as follows:

- 25°C 10 minutes
- 42°C 1 hour, 40 minutes
- 85°C 5 minutes

The cDNA was then used to perform qPCR. Triplicate reactions were prepared with 1.33µL of cDNA preparation, 20x TaqMan® gene expression assay for DACH1 (ABI®, Life Technologies™, Cat#: 4351372) and GAPDH (ABI® Life Technologies™, Cat# 4331182), 2x TaqMan® universal PCR master mix (No AmpErase® UNG), and nuclease-free water. 20µL samples were then plates and run on ABI® 7900HT Fast Real-Time PCR system using SDS version 2.3 software (ABI®), and the comparative Ct (Cycle threshold) ( $\Delta\Delta Ct$ ) method. Cycling conditions for qPCR were as follows:

- Stage 1 (HOLD) 95°C 10 minutes
- Stage 2(40 cycles) 95°C 15 seconds
- 60°C 1:00 minute

## 5.6 TaqMan® microRNA assays

Total RNA was prepared using an miRNeasy (microRNA extraction) kit (QIAGEN) and quantified, as previously described. Total RNA was diluted to 2ng/μL in RNase-free water, to give a final concentration of 10ng/μL total RNA per reaction. RNA for reverse transcription was prepared in singleplex reactions with miRNA-specific primers for miR-200b (target and RNU44 (internal control) and RNU48 (internal control) (ABI®, Life Technologies™, Cat#: 4427975). TaqMan® miRNA reverse transcription (RT) master mixes (ABI®, Life Technologies™) with MuLV RT were prepared as singleplex reactions using specific 5x RT primers specific for the miR-200b 3p strand, RNU44 and RNU48.

Per 15μL reaction using, 7μL of master mix was made up as follows

0.15μL of 100mM ddNTP

1.00μL of 50U/μL MultiScribe™ reverse transcriptase

1.50μL of 10x RT buffer

0.19μL of 20U/μL RNase Inhibitor

4.16μL RNase-free water

MasterMix and RNA were combined at a ratio of 7μL:5μL + 10%, with 7.7μL + 5.5μL.

12μL of MasterMix plus RNA was combined in a 0.2mL PCR tube, with 3μL of primer and gently mixed.

RT was carried out using recommended thermo cycling conditions:

On Ice 5 minutes

16°C 30 minutes

42°C 30 minutes

85°C 5 minutes

Reverse transcribed miRNA was then used to perform qPCR. These were set up in triplicate, with each individual reactions were prepared with 1.33 $\mu$ L of cDNA preparation (1:15 dilution), 1 $\mu$ L 20x TaqMan<sup>®</sup> microRNA expression assay for miR-200b, or 1.0 $\mu$ L of 20x TaqMan<sup>®</sup> microRNA expression assay for RNU44/RNU48 (ABI<sup>®</sup> Life Technologies<sup>™</sup>, Cat#: 4427975), 10.0 $\mu$ L 2x TaqMan<sup>®</sup> universal PCR MasterMix (No AmpErase<sup>®</sup> UNG), made to a final volume of 20L with 7.67 $\mu$ L of nuclease-free water. The 20 $\mu$ L samples were then plates and run on ABI 7900HT Fast Real-Time PCR system using ABI<sup>®</sup> SDS version 2.3 software (ABI<sup>®</sup>, ©2005), and the comparative Ct ( $\Delta\Delta$ Ct) method. Cycling conditions for qPCR were as follows:

Stage 1 (HOLD)	95°C	10 minutes
Stage 2(40 cycles)	95°C	15 seconds
	60°C	1:00 minute

All qRT-PCR data was collected using ABI<sup>®</sup> RQ manager version 1.2 software (ABI<sup>®</sup>, ©2005), and further analysed using Microsoft Excel.

## 5.7 Lentiviral Transductions

Transductions for the following were attempted:

- (i) Cell lines with low levels of mir-200b were transduced with a hsa-miR-200b-GFP-lenti reporter (Applied Biological Materials (ABM<sup>®</sup>) Inc., New York City, USA) (Cat#: Mh-15262).
- (ii) All cells were transduced with a DACH1-3'UTR-GFP-Lenti reporter virus (ABM<sup>®</sup> Inc., Cat#: MV-05537). See Figure 11a and 11b for vector constructs.

Protocol supplied by ABM<sup>®</sup> Inc. was followed, with adjustments made for optimisation.

Following the ABM protocol, cells were seeded the day before transfection at a density of  $0.5 \times 10^5$  cells per well.

On the day of transfection, cells were harvested and pelleted as usual, then resuspended in medium containing 8 $\mu$ g/mL of polybrene, and various amounts of viral medium were added. Also included were a GFP control lentivirus, and a negative control pLenti-III-Lentivirus

(ABM® Inc., Cat#: LVPS87) (Figure 11c). Controls for polybrene toxicity and another of uninfected cells were used as controls. Cells were incubated for 24 hours, then medium was removed and replaced with normal growth medium. Cells were incubated for a further 48 hours and then selected for with 2µg/mL of puromycin. A puromycin control was included.

Small adjustments were made to this, including cell numbers- cells were plated at a density such that they would be ~80% confluent, 72 hours after transfection (adherent cells were seeded at a density of  $1.4 \times 10^5$  cells/T25 flask (Nunc), and semi-adherent cells were plated at a density of  $\sim 1.0 \times 10^5$  cells/well in a 24-well plate (Nunc). Virus was also removed after 3-4 hours of incubation. Cells were allowed to recover for three days before selection.

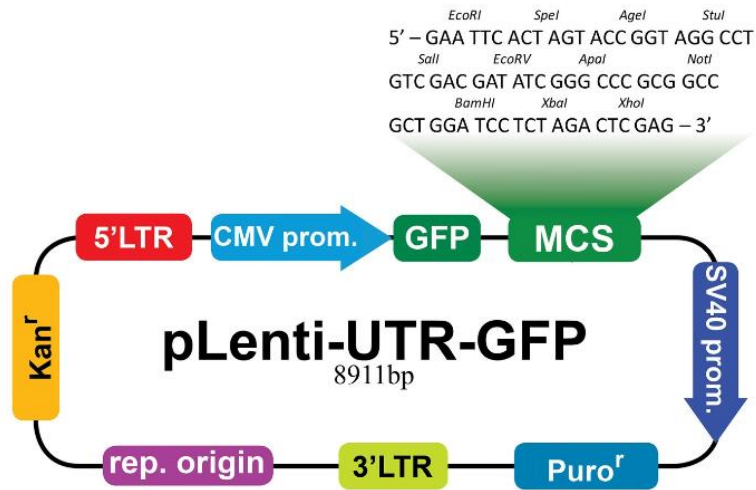


Figure 11a. DACH1-3'UTR-Lenti-reporter-GFP viral vector

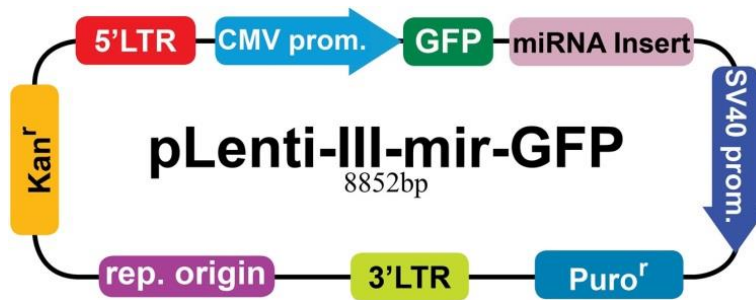


Figure 11b. Lenti-miRa-GFP-hsa-miR-200b viral vector

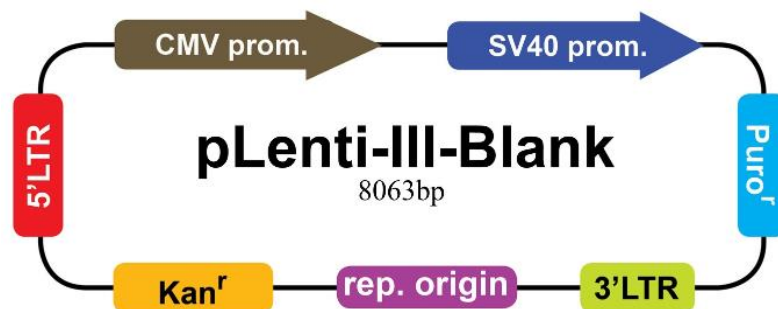


Figure 11c. pLenti-III-blank-lentiviral vector

Lentiviruses were obtained commercially from ABM® Inc. All three include a CMV promoter, and contain puromycin resistance ( $Puro^r$ ) gene for cell selection. DACH1-3'UTR-GFP-lenti reporter viruses also contain a Green fluorescent protein gene (GFP) linked to the DACH1 3'UTR for assessment of reporter expression with high or low miR-200b expression.

## 5.8 Cloning

### 5.8.1 Transformation of *E. coli*

One Shot® TOP10 chemically competent *E. coli* (Invitrogen™, Life Technologies™) were transformed with 2ng of DACH1 3'UTR lenti-reporter-Luc Vector plasmid (ABM® Inc, Cat#:MT-h05537) (Figure 12.). Briefly, cells were combined with plasmid and incubated on ice for 30 minutes, transferred to 42°C for 30 seconds, and then kept on ice for 2 minutes. For recovery, 250µL S.O.C medium was added and cells plus medium were transferred into a 15mL Falcon tube (BD Falcon) and incubated in a shaker at 250rpm, 37°C overnight.

Following overnight incubation, 50µL, 100µL, and 150µL of cells were plated on LB agar plates containing Kanamycin (50µg/mL) and incubated at 37°C overnight. Plates were then stored at 4°C.

Two separate colonies were picked and used to inoculate individual 15mL falcon (BD Falcon) tubes containing 2 mL of LB broth/50µg/mL Kanamycin. These cells were incubated on a shaker at 250rpm at 37°C overnight. 100µL of the overnight mini prep culture was added to a conical flask containing 100mL of LB/ 50µg/mL Kanamycin broth and cultured at 37°C overnight.

Following overnight culture, the cells were transferred into two 50mL falcon tubes and centrifuged 4000rpm for 10 minutes.

Plasmids from transformed cells containing the DACH1 3'UTR lenti-reporter-Luc plasmid (ABM® Inc.), and pre-prepared cells containing pCAG-KPGY Gagpol plasmid, pCAG-VSVG envelope plasmid, and pCAG-RTR revtat plasmid (supplied by Dr Jacqueline Whitehouse) were isolated using *Plus* midiprep kit (QIAGEN) high efficiency protocol. Plasmid DNA quality was then assessed using the nanodrop spectrophotometer (Thermo Scientific) and stored at -20°C.

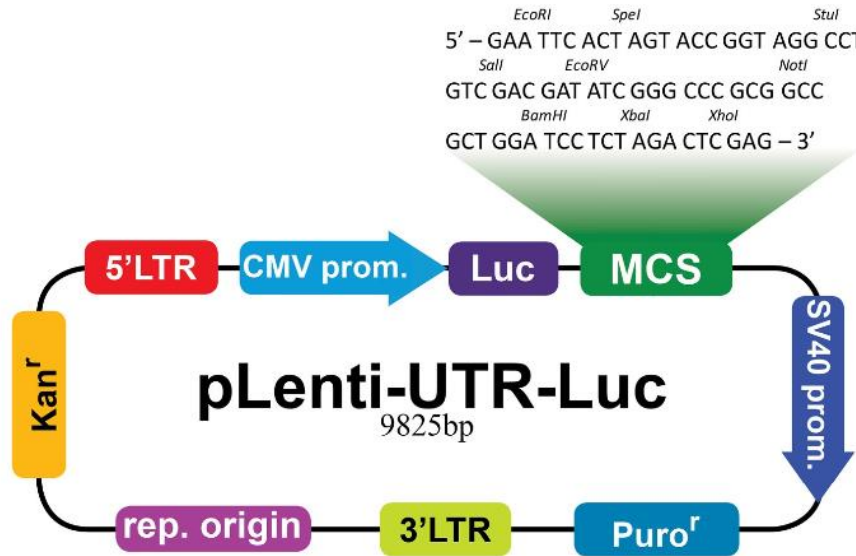


**Figure 12. pLenti-DACH1-3'UTR-Luc-reporter vector**

The pLenti-DACH13'UTR-luciferase-reporter vector was purchased from Applied Biological Materials Inc. (ABM). The vector contains a Kanamycin resistance ( $\text{Kan}^r$ ) gene used to select for transformed bacterial colonies, a Puromycin resistance ( $\text{Puro}^r$ ) gene for selecting transduced cells, and a luciferase reporter linked to the 3'UTR for assessing reporter expression in the presence of high and low levels of miR-200b.

## 5.9 Generation of lentivirus

To generate lentivirus, Human Embryonic Kidney 293T (HEK-293T) cells were transfected with reporter and packaging plasmids, according to the following procedure (supplied by Dr Jacqueline Whitehouse):

On day one,  $3 \times 10^6$  293T cells were plated in a 10cm culture dish with DMEM (Gibco®) + 1% (v/v) Penicillin/Streptomycin (pen/strep) (Gibco®) 1% (v/v) + 10% (v/v) FCS.

Day 2, plasmid DNA was combined in serum-free DMEM (Gibco®) and vortexed to mix. DNA was added at the following amounts:

12 $\mu\text{g}$  of vector plasmid (DACH1 3'UTR-lenti-reporter-Luc vector)

6 $\mu\text{g}$  of gagpol plasmid (pCAG-KPGY)

2µg of envelope plasmid (pCAG-VSVG)

2µg of revtat (pCAG-RTR)

FuGene 6® transfection reagent (Promega) was diluted in serum-free DMEM and vortexed to mix. FuGene and plasmid DNA were combined and added to cells with 8mL of fresh DMEM medium (Gibco®) + 1% Pen/Strep (Gibco®) + 1% Glutamax (Gibco®) + 10% FCS, and incubated 37°C for 24hours.

Day 3, media was removed and replaced with 5mL of DMEM medium (Gibco®) + Pen/Strep (Gibco®)+ Glutamax (Gibco®) + 10% FCS, and incubated 37°C/5% CO<sub>2</sub> for a further 24hours.

Day 4, 48 hours following transfection, the 48 hour viral supernatant was collected and stored on ice at 4°C overnight. 5mL of fresh DMEM medium (Gibco®) was added to cells.

Day 5, 5mL of 72 hour viral supernatant was collected and combined with 48 hour supernatant, and filtered through a 0.45µm filter syringe, then stored at -80°C.

## 5.10 Transfections

SiGlo green transfection indicator (Dharmacon, GE Healthcare, Cat#: D-001630-01-20), 20nmol dry stock, and *mirVana hsa-mir-200b-3p mimics* 5nmol dry stock (Ambion®, Life Technologies™, Cat#:4464066) were resuspended to a final concentration of 50µM, by adding 400µL, and 100µL of RNase-free water, respectively.

The Neon® electroporation system (Invitrogen, Cat#MPK5000) was use to conduct transfection, using 10µL Neon® tips (Invitrogen, Cat#MPK1096). 10µL of transfected cells were plated in 490µL of growth medium to a final volume of 500µL, in a 24 well plate. Optimal transfection conditions for D283 and D341 had previously been determined, with

successful transfection with 1 pulse at 1350 volts (V), 20 milliseconds (ms). These conditions were also found to be optimal for transfection of PER547 and D425.

Following the recommended protocol, cells were plated 1-2 days prior to transfection in normal growth medium. The following day cells were harvested and pelleted by centrifugation at 400xg for 5 minutes (ThermoScientific). Cells were counted on the countess (Invitrogen™), as previously described, and washed in PBS buffer (no MgCl<sub>2</sub>). Cells were resuspended in buffer R (Invitrogen™) to a density of 1.0x10<sup>7</sup> cells/mL, and mixed well to create a single cell suspension. 13μL aliquots of cell suspension were added with 2.6μL (or 6.5μL) of 50μM of hsa-mir-200b-3p *mirVana* mimic (Ambion®) (hereafter referred to ‘miR-200b mimic’) or miRNA negative control#1 (hereafter referred to as ‘control’) (Ambion®) and gently pipetted to mix. 10μL of cell mix was electroporated in 5mL of Buffer E (Invitrogen™) using conditions of 1350V, 1 pulse, 20ms. Electroporated cells were then plated in 490μL of pre-warmed culture medium, with miR-200b mimic/control at a final concentration of 20nM or 50nM). A total of 12 wells were plated for both the mimic and control. SiGlo was used as a transfection indicator to determine transfection efficiency. SiGlo (Dharmafect GE healthcare) was transfected to a final concentration of 20nM in 500μL using the same conditions.

Following 24-48 hour incubation, cell fluorescence of SiGlo (Dharmafect GE healthcare) transfected cells was assessed using the Tali™ image based cytometer (Invitrogen™). A control sample of un-transfected cells and a sample of SiGlo transfected cells were assessed. If cell fluorescence was >75%, transfected cells were harvested, and protein and RNA were extracted as described above, for downstream mRNA, miRNA, and protein analysis.

#### ***5.10.1 Lipofectamine® RNAiMAX transfection***

The recommended protocol was followed for transfection of DAOY cells using Lipofectamine® RNAiMAX Lipofectamine transfection (Invitrogen™, Cat#: 13778500).

In separate tubes, 9μL of RNAiMAX (Invitrogen™) or 1.2μL of 50nM SiGlo were diluted into 150μL of OptiMEM (Gibco®) reduced serum medium. 150μL of both diluted SiGlo and

RNAiMAX were combined in a 1:1 ratio and incubated at room temperature for 5 minutes to allow complexes to form. 250µL of combined solution was then added drop-wise to cells, into a final volume of 250µL, giving a final concentration of 20nM.

Cells were incubated for at least 24 hours and fluorescence was then assessed using the Tali™ image based cytometer (Invitrogen™) as described below.

### **5.10.2 Tali™ Image based cytometer**

Cells were harvested 24 hours following transfection and fluorescence was assessed by transferring a 25µL aliquot of cells onto a Tali™ slide (Invitrogen™). An un-transfected sample was assessed to obtain a background measure. Gates were set so that 0% fluorescence was detected in control un-transfected cells. Transfected cells were then assessed using Green fluorescent detection and a right hand shift of the curve indicated positive transfection. A percentage value of fluorescent cells was then obtained. Cells with  $\geq 70\%$  fluorescence were used for downstream expression analysis.

## **5.11 Data analyses**

### **5.11.1 qRT-PCR expression data**

qRT-PCR data was collected using ABI® RQ manager version 1.2 software, and exported to excel for analysis. Relative Quantitation ( $\Delta\Delta Ct$ ) analysis was performed, as previously described. Briefly, average Ct values from two to three independent experiments, with two to three replicates per-experiment were collected. Average Cts  $\geq 32$  were given a value of zero to represent no expression.

Normalised expression between the Gene of Interest (GOI), DACH1 and miR-200b, and the Internal control GAPDH, and RNU44/RNU48, was calculated as  $\Delta Ct$  value where  $\Delta Ct = Ct_{GOI} - Ct_{Internal\ Control}$ . For post-transfection analysis, the  $\Delta Ct$  was adjusted to  $2^{-\Delta Ct}$  and Log2 transformed to give a value representing normalised expression (target relative to control). For the base-line analysis, relative quantitation (RQ) was determined using D283 as a

normalised. This was calculated as  $\Delta\Delta Ct = \Delta Ct_{GOI} - \Delta Ct_{normaliser (D283)}$ , and adjusted  $2^{-\Delta\Delta Ct}$  and Log2 transformed.

Standard deviation (SD) was calculated as the SD between the target and control =  $(GOI SD^2 + internal\ control\ SD^2)^{0.5}$ . The Ct SD was presented as error bars.

### ***5.11.2 Western blot and protein quantification***

Membranes were probed with primary and secondary antibodies, and protein was detected using SuperSignal® WestDura Extended duration substrate (ThermoFisher Scientific). Immunoblots were visualised using the ChemiDoc MP imaging system (BioRad), and were presented in BioRad ImageLab 5.1 software.

Relative protein was determined by assessing the quantity of DACH1 to the  $\beta$ -actin control. Quantity was determined based on band intensity. Normalisation to  $\beta$ -actin was carried out as band intensity of DACH1 band-band intensity of  $\beta$ -actin band, and Log2 transformed.

## 6.0 RESULTS

### 6.1 An inverse correlation between DACH1 and miR-200b expression in medulloblastoma cell lines

The DACH1 3'UTR contains a putative binding site for miR-200b (see Figure 10.) suggesting that miR-200b may target the DACH1 transcript. To address this, miR-200b and DACH1 expression were assessed in six medulloblastoma cell lines, using two-step quantitative reverse transcription polymerase chain reaction (qRT-PCR). Ct values  $\geq 32$  were considered negligible or no expression. An inverse correlation between levels of DACH1 mRNA and miR-200b was detected in 5/6 cell lines, with D425 being the exception (Figure 13.).

For analysis, expression was normalised against an internal control; GAPDH was the internal control used for normalisation of DACH1 expression in all cell lines, RNU44 was used as an internal control for miR-200b in D341, PER547, and D283, while RNU48 was an internal control in D425. D425 was normalised to the internal control RNU48 due to RNU44 having higher Cts compared to the other cell lines. RNU48 also had higher Ct values than RNU44 in the other five cell lines, skewing the normalisation of D425. Original, un-normalised Ct data (Appendix B.) demonstrates that miR-200b expression is relatively consistent across all cell lines, including D425.

The comparative Ct ( $\Delta\Delta Ct$ ) method was used for normalisation of expression, presented as DACH1 or miR-200b expression normalised to the appropriate internal control, and relative to D283 cell line. This method was previously described by (Livak & Schmittgen, 2001; Schmittgen & Livak, 2008). Figure 13 presents the normalised levels of DACH1 and miR-200b in each of the cell lines that were investigated. A summary of their expression is presented in Table 3.

DACH1 protein was detected using western blot to confirm expression at the protein level. Consistent with the qRT-PCR data, a prominent band of ~97kDa, the predicted size of the DACH1 protein was detected in PER547 and D341, and lower levels of DACH1 protein were present in D425 and D283. DACH1 protein was not detected in DAOY or UW228

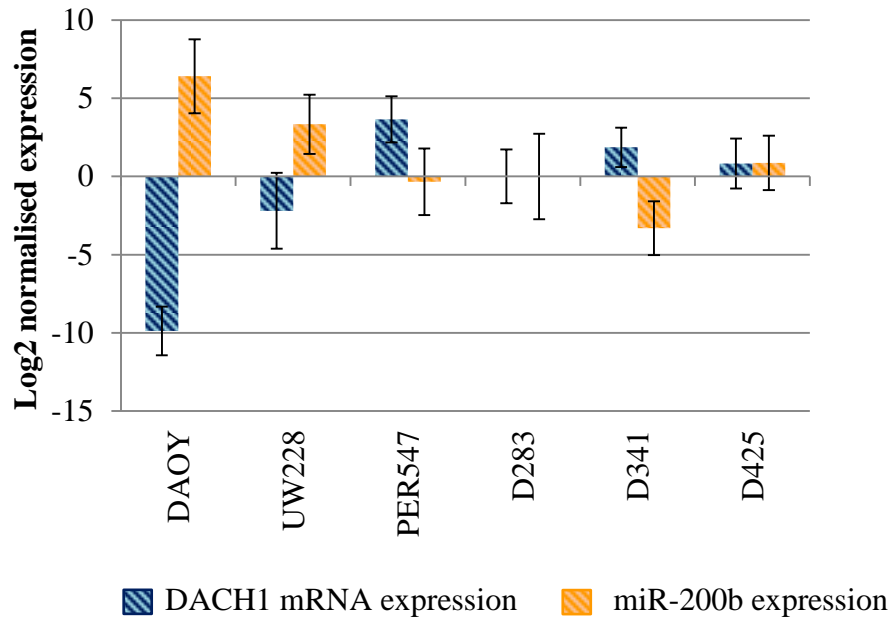


**Figure 13. Expression of DACH1 and miR-200b in medulloblastoma cell lines, relative to D283.**

An inverse correlation between the expression of DACH1 mRNA and miR-200b was evident in the majority of cell lines (5/6). Total RNA and miRNA-enriched RNA were extracted from all cells, and expression was assessed using qRT-PCR. Each extraction was repeated three times, with two to three replicates for each cell line for each qRT-PCR experiment. The results were analysed using relative quantitation, with average cycle threshold (ct) values normalised against a respective internal control; for DACH1, GAPDH was used as the internal control in all cell lines, and for miR-200b, RNU48 was used as an internal control for D425, while RNU44 was used as the internal control for the remaining cell lines. Normalised expression was determined relative to D283.

To highlight the inverse correlation, no cut-off ct value was applied here, however DACH1 expression in DAOY, and miR-200b expression in PER547, D283, D341, and D425 all had ct values  $\geq 32$ , which was designated as ‘no expression’. The error bars represent standard deviation (SD) between ct values from each independent experiment. SD was calculated as  $(SD \text{ DACH1}^2 - SD \text{ GAPDH}^2)^{0.5}$  or  $(SD \text{ miR-200b}^2 - SD \text{ RNU44/48}^2)^{0.5}$ .

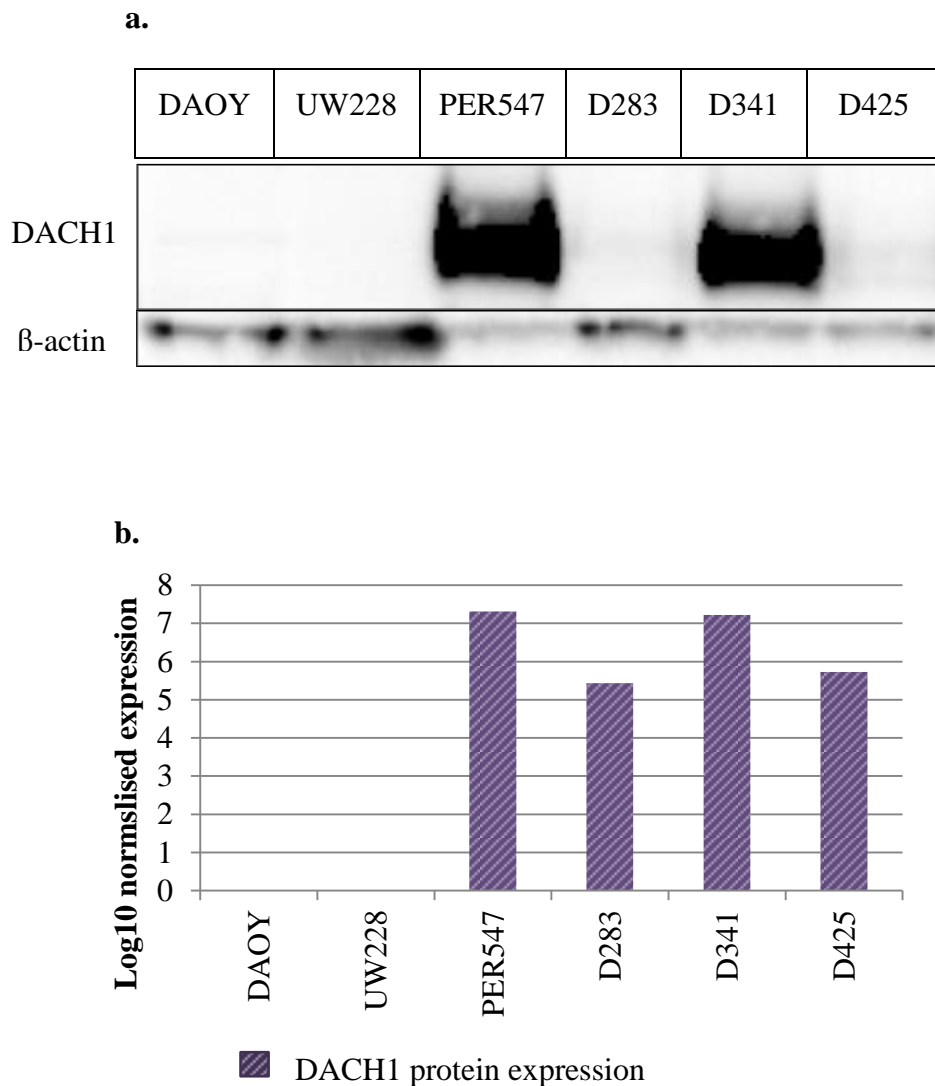


**Figure 14. DACH1 protein expression in six representative medulloblastoma cell lines with quantitative analysis of protein expression**

(a.) DACH1 protein was detected in the four cell lines that also showed elevated DACH1 mRNA expression, and was not detected in DAOY and UW228.  $\beta$ -actin was used as a loading control, and indicated that higher levels of protein were loaded for DAOY, UW228, and D283. (b.) Additional quantitative analysis of DACH1 protein expression was performed, relative to  $\beta$ -actin. PER547 and D341 expressed high levels of DACH1, D425 and D283 expressed lower levels, while no DACH1 protein was detected in DAOY and UW228.

**Table 3. Simplified summary: an inverse correlation exists between DACH1 and miR-200b**

	<b>DACH1</b>	<b>miR-200b</b>
<b>DAOY</b>	Low	High
<b>UW228</b>	Low	High
<b>PER547</b>	High	Low
<b>D283</b>	High	Low
<b>D341</b>	High	Low
<b>D425</b>	High	Low

A summary of DACH1 and miR-200b expression, showing an inverse correlation between DACH1 and miR-200b that is based on average Ct data (Appendix B).

## **6.2 Addressing the inverse correlation between DACH1 and miR-200b**

### ***6.2.1 Stable transductions with Lentivirus***

Lentiviral transductions using commercially obtained lentiviruses DACH1 3'UTR Lenti-Reporter-GFP virus, and Lenti miRa-GFP-hsa-mir-200b virus (Applied Biological Materials Inc. (ABM)) were attempted in cell lines with low endogenous miR-200b expression. However, due to unexpected problems with commercially purchased DACH1-3'UTR-GFP-Lenti reporter viruses, reporter cell lines were not generated. This was due to evidence of bacterial contamination of viral stocks. Contamination was suspected following high levels of cell death occurring 72-96 hours after transductions but prior to puromycin selection. Importantly, this occurrence was only identified in cells that were inoculated with the purchased lentivirus.

To further confirm the source of contamination, culture medium was inoculated with viral medium, and produced visible growth of bacteria 72-96 hours after inoculation, which was not detected in medium alone. Cells were cultured in 1% Penicillin/Streptomycin and maintained post-transduction however this did not prevent outgrowth of bacteria. Consequently a new approach was needed in order to assess the potential association between DACH1 and miR-200b.

DACH1-3'UTR-Luc-lenti reporter plasmids (Figure 12.) were purchased from ABM Inc. and used to generate lentiviruses. DAOY cells proved easy to transduce and produced puromycin-resistant colonies. This indicated that the virus was capable of infecting cells and was then applied to semi-adherent cells with low miR-200b expression. These cells proved difficult to transduce and puromycin resistant colonies were not detected after repeat attempts. Due to time constraints, this protocol was not optimised, and therefore no data were collected.

### ***6.2.2 Transient transfection of selected medulloblastoma cell lines***

The difficulties associated with the viral transduction strategy described above, necessitated an alternative approach for the manipulation of miR-200b levels in medulloblastoma cell lines. A second approach to assessing whether DACH1 was targeted by miR-200b involved transient transfection of mir-200b mimic and antagomirs. Cell lines with low levels of

DACH1 expression, and high levels of miR-200b expression based on raw Ct values (Appendix B), were to be transfected with miR-200b antagomirs, however, as described in section 6.2.5, no optimised protocol was developed for these cell lines and transfection with miR-200b antagomirs was not conducted. Cell lines with high levels of DACH1 expression, and low miR-200b expression based on raw Ct values (Appendix B), were selected for further analysis. These cell lines included D341, D425, PER547, and D283.

Firstly, optimal transfection conditions were tested for PER547 and D425, while previously optimised conditions were available for D283 and D341. Transfection conditions used for D283 and D341 also produced the highest transfection efficiency in PER547 and D425. To determine transfection efficiency, cells were transfected with SiGlo fluorescent green transfection indicator at a final concentration of 20nM, and fluorescence was assessed following a 24 hour incubation. Further analysis was performed when transfection efficiency of SiGlo control cells was  $\geq 75\%$ .

Cells were transiently transfected with a final concentration of 20nM of hsa-mir-200b-3p *mirVana* mimic or miRNA negative control#1, and a final concentration of 50nM of hsa-mir-200b-3p *mirVana* mimic or miRNA negative control#1.

Protein and miRNA-enriched RNA were extracted at both 24 hours and 48 hours post-transfection, for expression analysis.

### ***6.2.3 Confirming miR-200b expression post-transfection***

qRT-PCR was used to confirm whether miR-200b expression was restored following transient transfection of these cell lines. Successful restoration of miR-200b expression was confirmed following transfection with 50nM and 20nM mimic, by calculating Ct averages for miR-200b and RNU44/RNU48, and normalising miR-200b expression to RNU44 (RNU48 in D425) to obtain a  $\Delta Ct$  value for mir-200b mimic, and negative control transfected cells.

Normalised miR-200b expression in cells transfected with mir-200b mimic was compared to the corresponding cell line transfected with negative control#1. These data were presented as Log2 transformed  $2^{-\Delta Ct}$  values.

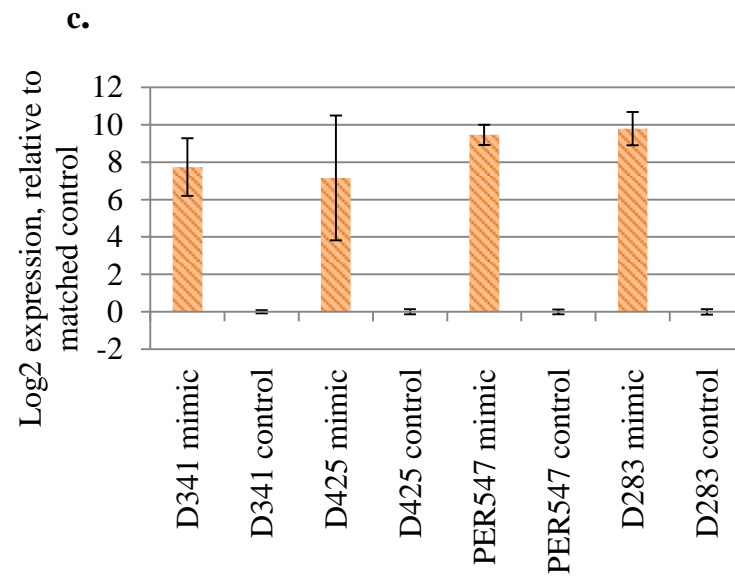
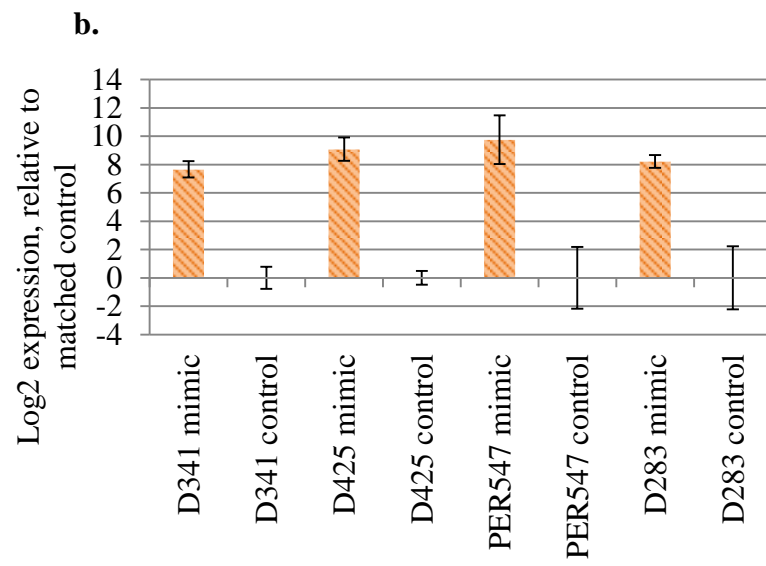
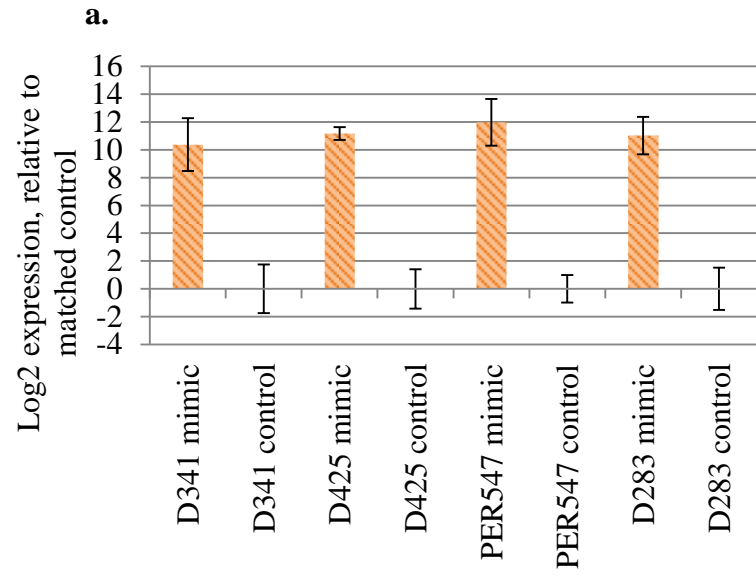
#### ***6.2.4 Determining inhibition of DACH1 by miR-200b***

To address the predicted targeting of DACH1 by miR-200b, hsa-mir-200b-3p stem loop *mirVana* mimics were transiently transfected into 4/6 medulloblastoma cell lines with low endogenous miR-200b, and relatively high DACH1 mRNA and protein (Table 3.). Two concentrations were selected; 50nM and 20nM

#### ***6.2.5 Optimising transfection of adherent medulloblastoma cell line***

The adherent cell lines DAOY and UW228, had higher levels of miR-200b expression and lower DACH1 expression based on raw Ct values (Appendix B.), and therefore were selected for transfection with hsa-mir-200b-3p *mirVana* antagomirs (mir-200b antagomirs).

Identification of optimal NEON transfection conditions for DAOY and UW228 cell lines was attempted using 5-20nM SiGlo as an indicator of positive transfection. Optimisation was attempted using conditions recommended by the manufacturer, however cells proved difficult to transfect using this method, with transfection efficiency between 2-30% positive cells, depending on the conditions used. The reasons for low transfection efficiencies using this approach were unclear, and no optimised protocol using the NEON was generated. As an alternative, transfections were attempted using the lipofectamine-based RNAiMAX. The recommended protocol was followed, however transfection was unsuccessful. Due to time constraints an optimised protocol was not developed, and consequently transfection of mir-200b antagomirs could not be completed.



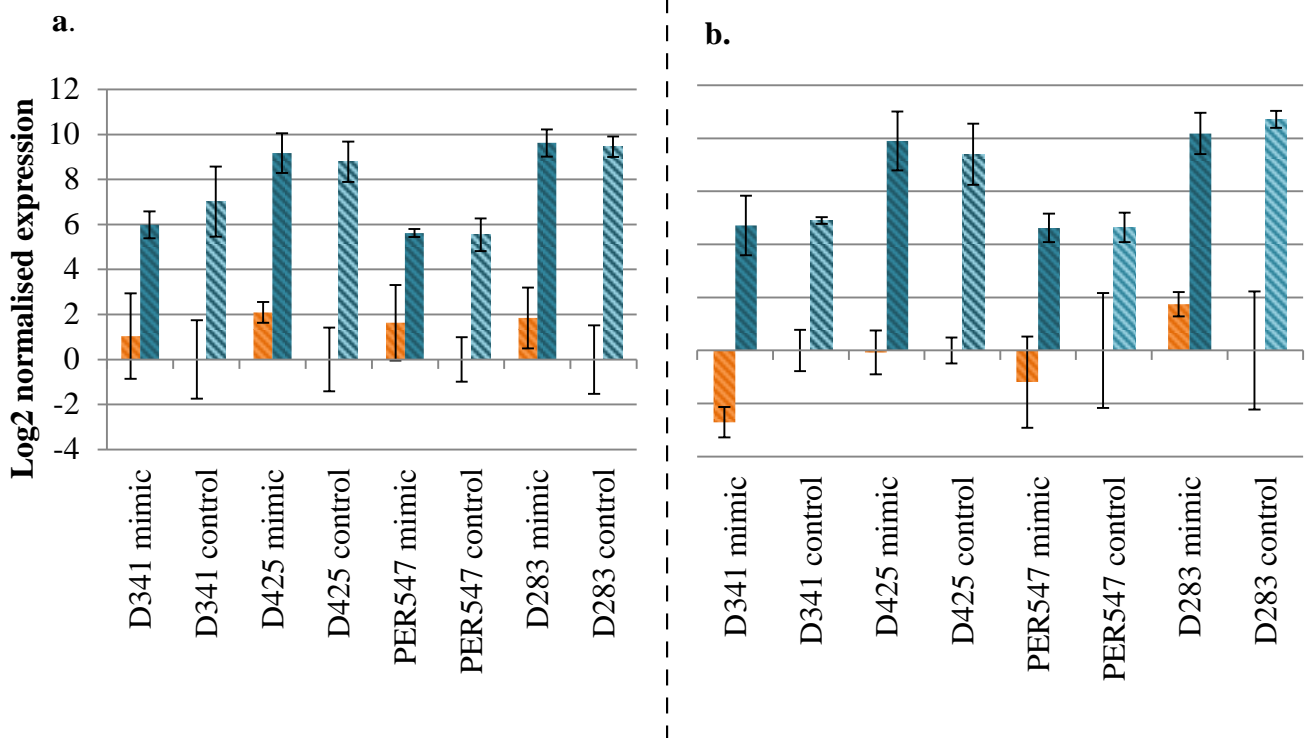
-  miR-200b expression following transfection with hsa-miR-200b mimic
-  miR-200b expression following transfection with negative control#1

**Figure 15. Successful transient transfection of cell lines with 20nM and 50nM of hsa-mir-200b-3p mimic, confirmed by qRT-PCR**

miRNA enriched RNA was extracted from four cell lines, 24 and 48 hours post-transfection with 20nM of either hsa-mir-200b-3p *mirVana* mimic (mir-200b mimic) or miRNA negative control#1 (control). qRT-PCR was performed to assess miR-200b expression post-transfection with mir-200b mimic, relative to matched control cells transfected with the control. (a.) miR-200b expression in cell lines, 24 hours post-transfected with 20nM of mir-200b mimic. (b.) miR-200b expression in cell lines, 48 hours post-transfection with 20nM of mir-200b mimic. (c.) miR-200b expression in cell lines, 24 hours post-transfection with 50nM mir-200b mimic.

Expression was normalized against RNU44 as the internal control for D341, PER547, and D283, and RNU48 as the internal control for D425. Average cycle threshold values (Cts) were included from two independent transfection with three replicates each, with Ct values  $\geq 32$  being considered as no expression, to eliminate the possibility of detecting background noise. The relative quantity of normalised miR-200b expression in cells transfected with mir-200b mimic was compared matched control cell line transfected with negative control. Transfections successfully restored miR-200b levels in all cells transiently transfected with mir-200b mimic.

Change in expression is presented as hsa-mir-200b-3p mimic transfected cells relative to the matched miRNA negative control#1 transfected cells ( $2^{-\Delta\Delta C_t}$ ). The error bars represent standard deviation between Ct values for each cell line (Ct SD calculated as  $(SD\ mimic^2 + SD\ control^2)^{0.5}$ ).



**Expression post-transfection with hsa-miR-200b-3p mimic**

■ DACH1 mRNA expression  
 ■ miR-200b expression

**Expression post-transfection with miRNA negative control #1**

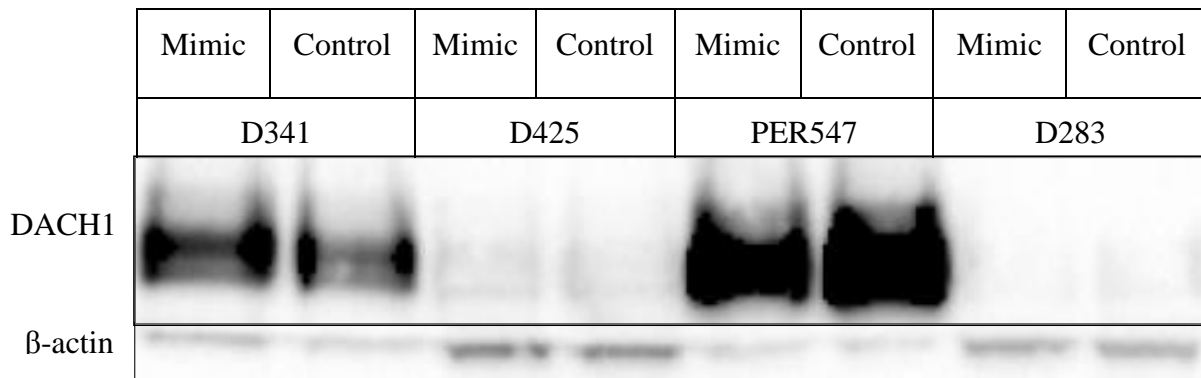
■ DACH1 mRNA expression  
 ■ miR-200b expression

**Figure 16. DACH1 mRNA expression is not affected by miR-200b expression in cells transiently transfected with 20nM of miR-200b mimic, at 24 hours and 48 hours post-transfection.**

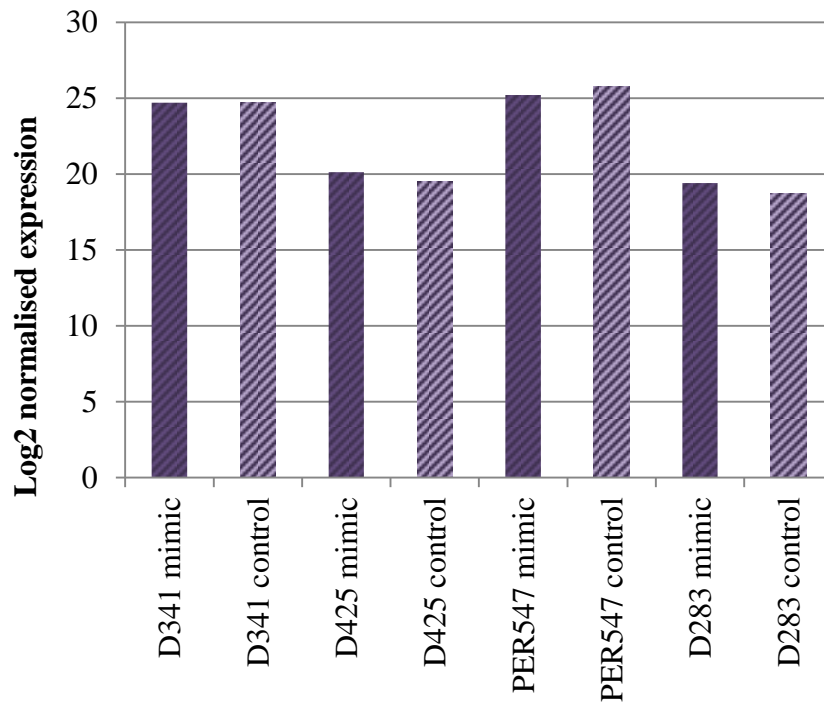
Cell lines were transfected with 20nM of mir-200b mimic or 20nM of control. Two independent transfections were performed, and miRNA-enriched mRNA was extracted for analysis at 24 hours and 48 hours post-transfection. Both DACH1 mRNA and miR-200b expression were assessed in cell lines transfected with miR-200b mimic and control, using qRT-PCR. Each qRT-PCR reaction was performed in either duplicate or triplicate, and average Ct values were analysed, using GAPDH, RNU44, and RNU48 as internal controls. Normalised expression of miR-200b is presented as Log2 transformed  $2^{-\Delta Ct}$ , and normalised expression of DACH1 is presented as Log2 transformed  $2^{\Delta Ct}$ . Error bars represent Ct SD; (Ct SD calculated as  $(SD\ mimic^2 + SD\ control^2)^{0.5}$ ).

Mir-200b expression did increase, however no change in the DACH1 mRNA levels was observed at either time point.

a.



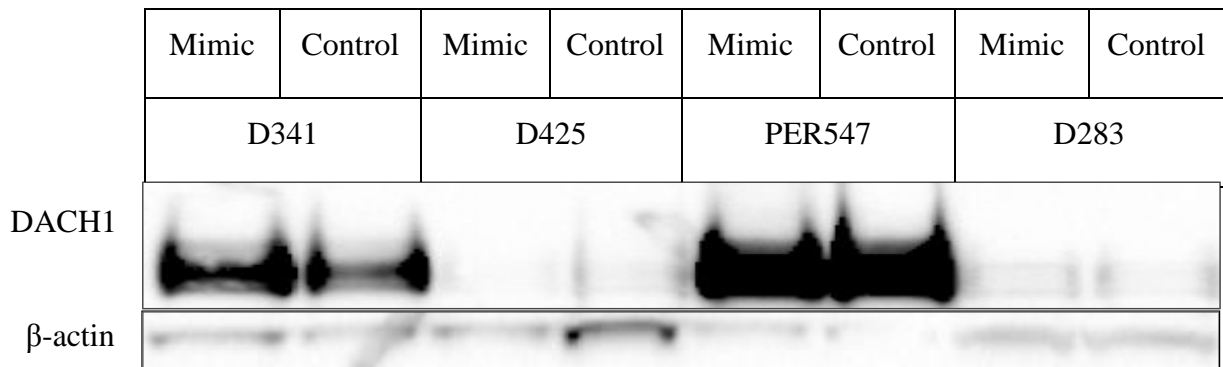
b.



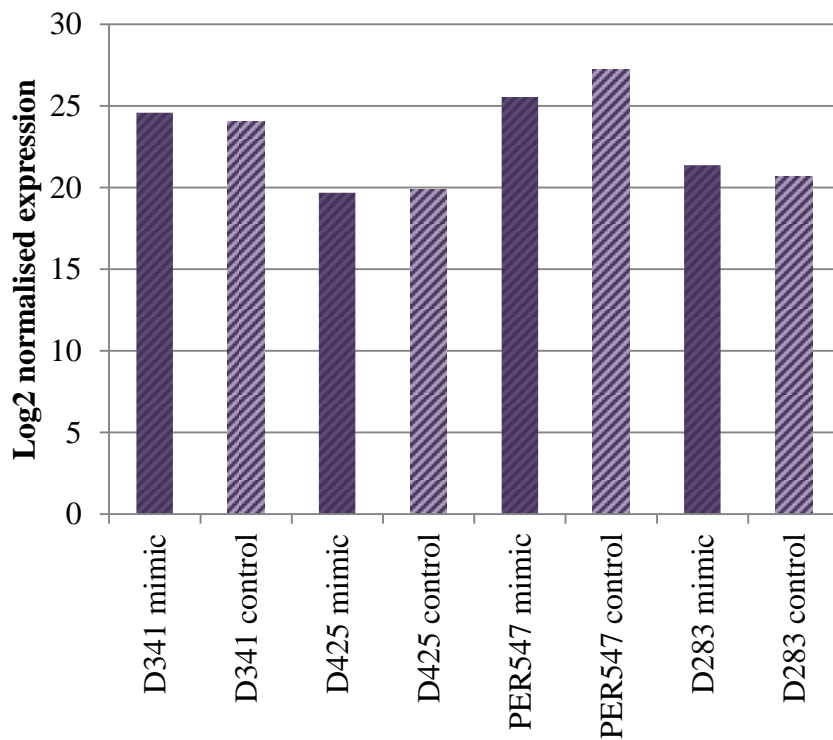
■ DACH1 protein expression in cells transfected with hsa-miR-200b-3p mimic

▨ DACH1 protein expression in cells transfected with miRNA negative control #1

c.



d.

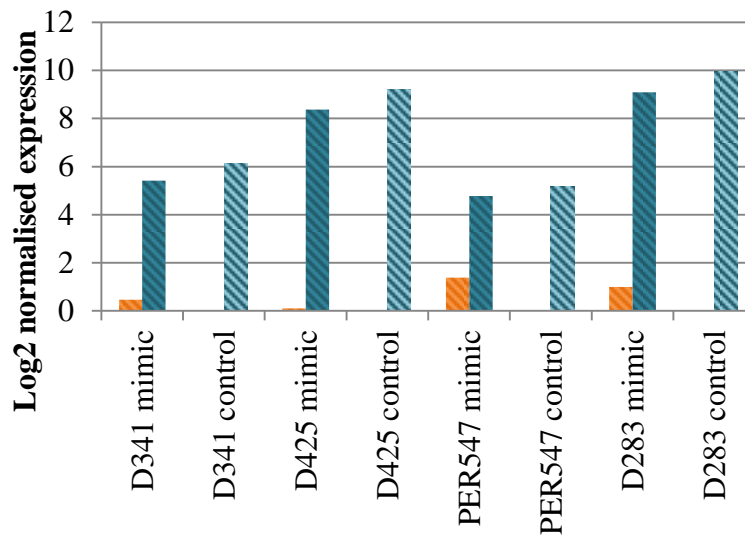


- DACH1 protein expression in cells transfected with hsa-miR-200b-3p mimic
- ▨ DACH1 protein expression in cells transfected with miRNA negative control #1

**Figure 17. DACH1 protein expression does not appear to be translationally repressed in cells transiently transfected with 20nM of miR-200b mimic, compared to cells transfected with 20nM of control, at 24 and 48 hours post-transfection.**

Protein lysate was collected from cells transfected with 20nM of mir-200b mimic or control, at (a.) 24 hours and (c.) 48 hours post-transfection. Western blot was used to detect protein expression and determine if DACH1 protein expression was down-regulated following restoration of miR-200b expression. Bands were detected at 97kDa- the expected size of the full length DACH1 protein, and did not appear to show reduced intensity in cells transfected with miR-200b mimic compared to cells transfected with the control at either time point.  $\beta$ -actin was used as the loading control, and showed relatively even loading across all lanes.

Quantitative analysis was then performed for protein expression (b.) 24 hours and (d.) 48 hours post-transfection, with DACH1 band intensity normalised against  $\beta$ -actin band intensity in miR-200b and control-transfected cells, then Log2 transformed. Quantitative analysis also did not indicate significantly reduced DACH1 expression at either time point.



**Expression post-transfection with hsa-miR-200b-3p mimic**

- DACH1 mRNA expression
- miR-200b expression

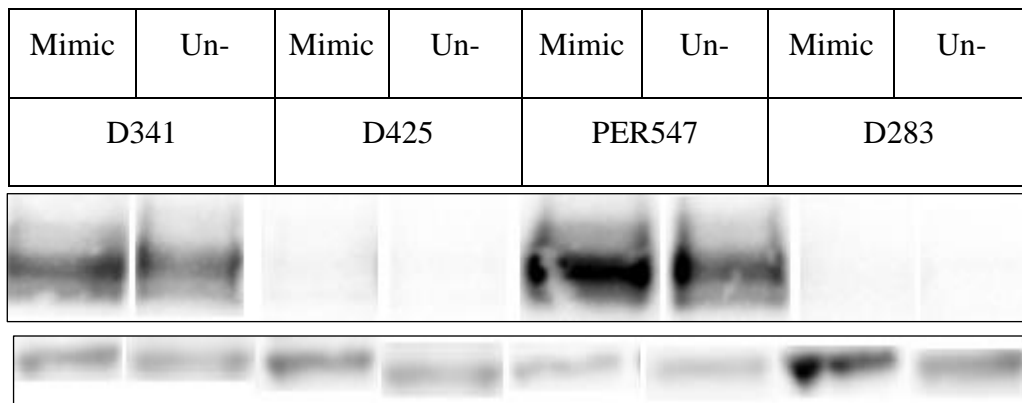
**Expression post-transfection with miRNA negative control #1**

- DACH1 mRNA expression
- miR-200b expression

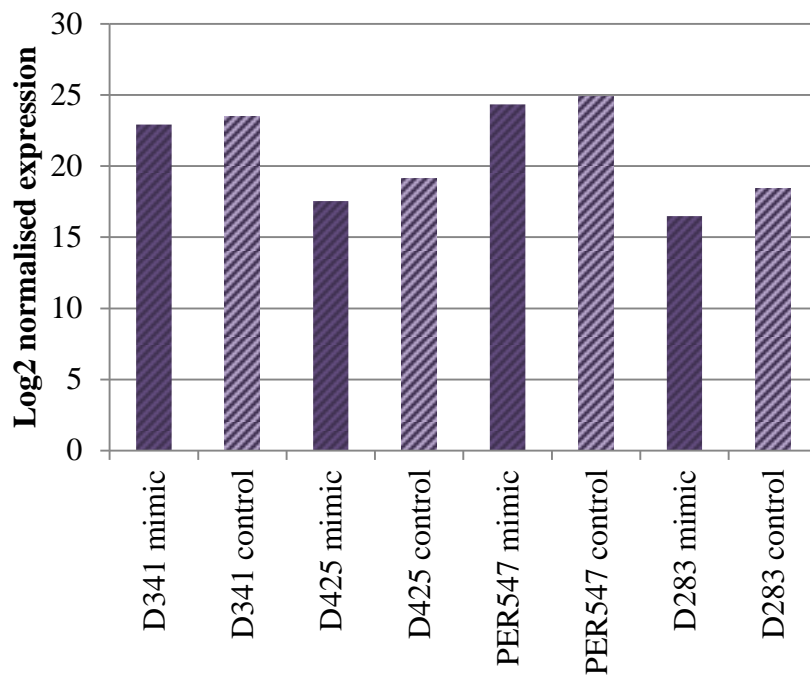
**Figure 18. DACH1 mRNA expression is not affected by miR-200b in cells transiently transfected with 50nM hsa-mir-200b-3p mimic at 24 hours post-transfection.**

50nM of mimic was transfected into four representative cell lines and miRNA enriched RNA was extracted at 24 hours post transfection for expression analysis using qRT-PCR to determine miR-200b and DACH1 mRNA expression relative to RNU44/48 and GAPDH. Two independent experiments were performed, and two to three replicate were performed. Ct values from replicates in both experiments were averaged and normalised against the appropriate internal control, then Log2 transformed. At this time point and this concentration, DACH1 levels remained relatively unchanged in cells transfected with mir-200b mimic, compared to those transfected with the control.

a.



b.



- DACH1 protein expression in cells transfected with hsa-miR-200b-3p mimic
- ▨ DACH1 protein expression in cells transfected with miRNA negative control #1

**Figure 19. DACH1 protein expression does not appear to be translationally repressed in cells transiently transfected with 50nM of miR-200b mimic, compared to un-transfected cells, at 24 hours post-transfection**

(a.) Protein lysate was collected from un-transfected cells (Un-), and cells transfected with 50nM of mir-200b mimic 24 hours post-transfection, and used for western blot analysis to detect DACH1 protein expression, and assess for any variation in expression. A band at approximately 97kDa was detected, and indicates reduced band intensity in cells transfected with miR-200b as compared to the un-transfected control.  $\beta$ -actin was used as a loading control with relatively even amounts of protein present in each lane (b.) For quantitative analysis, the intensity of DACH1 bands were normalised against intensity of the internal control  $\beta$ -actin, and then Log2 transformed. Quantitative analysis also suggests a reduction in DACH1 at the protein level, in cells transiently transfected with mimic.

## 7.0 DISCUSSION

### 7.1 DACH1 and miR-200b expression are inversely correlated in medulloblastoma cell lines

DACH1 expression has not previously been specifically investigated in medulloblastoma, but previous genome-wide transcriptional profiling indicated elevated expression of DACH1 relative to normal cerebellum in all four medulloblastoma sub-groups. Notably, DACH1 expression was significantly higher in Group 4 relative to the other three sub-groups (Mark Remke, University of Toronto. Pers comm). DACH1 mutations were not detected in medulloblastoma genome sequence analyses (Parsons et al., 2011; Robinson et al., 2012) and rarely identified in analyses of other cancers (COSMIC database, COSG74875). This suggests a potential oncogenic role of epigenetic up-regulation of DACH1 expression, such as by reduced DNA methylation (Hovestadt et al., 2014). Analysis of miRNA expression in a small panel of human medulloblastoma specimens performed in the Brain Tumour Laboratory at the Telethon Kids Institute, indicated that miR-200b was down-regulated in Group 4 medulloblastoma (Genovesi et al., 2011). Similar to DACH1, reduced expression of miR-200b may be a consequence of altered epigenetic mechanisms causing promoter hypermethylation affecting miR-200 family cluster and miR-200b, which is frequently down-regulated in cancer. This reduced expression is associated with early stages of metastasis linked to de-regulated EMT (Feng et al., 2014). Here it was predicted that DACH1 was regulated by miR-200b and that elevated DACH1 was a result of reduced miR-200b expression, potentially associated with the increased metastatic propensity of Group 4 medulloblastoma.

Additional *in silico* analysis of the 3'UTR of DACH1 using the TargetScan algorithm identified potential binding sites for nine miRNAs/clusters. Of these, the miR-200b/c/429 cluster was identified as having high probability of binding with a predicted 8-mer binding site from nucleotides 971-978 (Figure 10a and 10b). These correlative data are suggestive of DACH1 being a target of miR-200b. To address this possibility *in vitro*, DACH1 and miR-200b expression were assessed in six medulloblastoma cell lines. The results demonstrated an inverse correlation between DACH1 and miR-200b in these cell lines. Specifically, we showed that in cell lines with elevated DACH1, miR-200b was reduced, and vice versa (Figure13.). Western blot analysis for DACH1 protein expression in these cell lines was

consistent with DACH1 expression at the mRNA level, and was inversely correlated with miR-200b expression. This further supported the potential relationship between the expression of DACH1 and miR-200b.

The elevated DACH1 expression observed in four of our cell lines representing Group 3 medulloblastoma is consistent with previous studies that showed a significant increase in DACH1 levels in all sub-groups of medulloblastoma, particularly Group 3 and Group 4, relative to normal cerebellum. It can be speculated that this elevated expression may be a consequence of deregulated epigenetic mechanisms, such as reduced methylation of the DACH1 promoter or regulatory elements. This has been suggested previously (Hovestadt et al., 2014). Regulation by microRNAs is another possibility, given that there are numerous over and under-expressed microRNAs involved in medulloblastoma pathogenesis. Members of the miR-200 family in particular are of interest, given their well-described role in metastatic cancers (Park et al., 2008; Zhang & Ma, 2012), and putative binding site within the DACH1 3'UTR. Tentatively, reduced expression of miR-200b would correspond with the metastatic phenotype of Group 4 medulloblastoma (Davalos et al., 2012). Both DACH1 and miR-200b are linked with EMT, through the regulation of the transcription factors Snail and ZEB (Barry et al., 2008; K. Wu, Chen, K., Wang, C., et al., 2014), ultimately controlling E-cadherin expression (Davalos et al., 2012).

It is important to note here that our experiments were carried out using cell lines representing Group 3 medulloblastoma, rather than Group 4. However, it is evident that some Group 3 tumours expressed higher levels of DACH1. Additionally, an association was still seen between DACH1 and miR-200b levels. This suggests that a potential relationship between DACH1 and miR-200b also exists in Group 3 medulloblastoma, however, there may be underlying differences in the mechanisms associated with altered expression

To our knowledge, DACH1 has not yet been verified as a target of miR-200b in any context. Here, we speculate that in medulloblastoma, DACH1 is a target of miR-200b, and that reduced miR-200b results in elevated DACH1, and this may be linked to Group 4 medulloblastoma pathogenesis. This warranted further investigation to determine whether DACH1 is a bona-fide target of miR-200b.

## **7.2 Stable lentiviral transduction to generate reporter cell lines**

To address whether DACH1 is a bona fide target of miR-200b, we attempted to transduce our medulloblastoma cell lines with a DACH1-3'UTR-GFP-Lenti reporter virus, to confirm direct targeting by miR-200b. However, issues with contamination of commercial viral stocks prevented these experiments from being carried out. Initially, the high amount of cell death observed following transduction was assumed to be due to poor transduction efficiency, resulting in low numbers of puromycin resistant cells. Optimisation experiments were carried out using different viral MOIs and longer recovery times following transduction, in attempt to improve cell viability. It was observed that cell death was occurring prior to puromycin selection. Bacterial contamination was suspected given that both the untransduced control cells, and positive controls containing a GFP control lentivirus generated within our lab, showed no evidence of contamination and the source was traced to the viral stocks. To confirm, all components/reagents used for transductions, including fresh vials of virus, were inoculated into medium and incubated at 37°C for 72-96 hours. Bacterial outgrowth was detected only where viral media was inoculated, confirming contamination of viral stocks purchased from a commercial source.

Subsequently, we generated our own lenti-reporter virus containing DACH1-3'UTR-Luciferase-plasmid purchased from ABM. Inc. (the same supplier of the original viruses). Our lentivirus successfully transduced DAOY cells and generated puromycin resistant colonies. However, transduction of semi-adherent medulloblastoma cell lines was unsuccessful. The reasons for this were unclear, and further experiments were abandoned due to time constraints. Possible explanations include a low viral MOI, not sufficient for transducing cells; the slower proliferation rates of the semi-adherent cell lines, or the tendency for these cells to aggregate reducing surface area available for viral transduction. For future investigation/experiments, an alternative optimised protocol is required.

## **7.3 Transient transfection to alter miR-200b levels**

In the meantime, an alternative approach was used to investigate whether restoring miR-200b expression had any effect on DACH1 mRNA/protein expression. Cells with low levels of miR-200b expression were transiently transfected with a single hsa-miR-200b-3p mimic to restore miR-200b levels, followed by analysis of DACH1 mRNA and protein expression.

Two concentrations (20nM and 50nM) of hsa-miR-200b-3p mimic (miR-200b mimic) and miRNA negative control#1 (control) were selected, and post-transfection analysis was performed 24 and 48 hours post-transfection. Transfection efficiency was confirmed based on an increase in detectable mir-200b mimic compared to cells transfected with the control. Although transfection of mir-200bmimic successfully increased miR-200b to detectable levels, post-transfection analysis of DACH1 mRNA did not reveal any noticeable difference in expression at either time point. However, given that translation repression may occur even when mRNA remains stable (Djuranovic, Nahvi, & Green, 2012; Selbach, Schwanhausser, & Thierfelder, 2008), DACH1 protein was assessed by western blot, to determine if translation repression was evident. At both 24 and 48 hours post transfection, with 20nM of mimic/control, no decrease in DACH1 protein was detected. Using 50nM of mimic, there was some indication of protein repression in mimic-transfected cells compared to un-transfected cells, as determined by visual analysis. Unfortunately, no repeat experiment was performed for confirmation due to time constraints.

Others have demonstrated successful inhibition of target following transfection of miR-200b mimics (Hailin et al., 2013; Ye et al., 2014), however we were unable to show down-regulation of DACH1 following transfection with a mir-200b mimic. This is suggestive that miR-200b is not capable of regulating DACH1 expression, however it would be premature to make this assumption without additional experiments.

Reporter screening would be ideal, and would provide a more conclusive indication of any potential interaction (Thomson, Bracken, & Goodall, 2011). Such experiments would involve the development of reporter cell lines, and assessing reporter activity relative to the amount of miR-200b expressed. Subsequently assessing reporter expression after transfection of mir-200b mimics and antagomirs would provide evidence of miR-200b directly interacting with the putative target within the DACH1 3'UTR. Furthermore, generating lentiviruses with mutations to the putative binding site, and assessing changes in reporter expression, in a similar fashion as described above, would provide direct evidence of whether miR-200b targets the DACH1 3'UTR directly. Evidence of miR-200b binding to the DACH1 3'UTR could then be confirmed by transfection of mimics and assessment by qRT-PCR and western blot, similar to what is described here.

In addition, regarding experimental design, which involved only two time points (24 and 48 hours), it is possible that any detectable changes occurred outside of this range. A broader range, with earlier time points (6-12 hours) and later time points (72 hours), would allow a more comprehensive assessment of any potential changes in DACH1 expression. In the long-term, this could be enhanced by the use of a lentiviral vector to stably maintain up regulation of miR-200b. Similarly, the amount of mimic used may need to be adjusted for any effects to be observed.

It is also acknowledged that assessing only one microRNA, miR-200b, may be a limited approach. It is likely that the regulation of DACH1 is more complex, involving additional miRNAs, particularly those of the miR-200 family sharing the same seed sequence (miR-200c, and miR429). Including additional members of the miR-200 family, both individually and in combination, would be an ideal approach.

Another possibility is that there may be alterations within the 3'UTR that abrogate miR-200b binding. Although this was not investigated here, it has been previously demonstrated that during oncogenic transformation, a gene's 3'UTR may become truncated or elongated, enabling a gene to escape miRNA regulation (L. Li et al., 2014; Lianoglou, Garg, Yang, Leslie, & Mayr, 2013). As the mRNA sequence of DACH1 in our cell lines was not examined, this would be an interesting concept for further investigation.

#### **7.4 TaqMan qRT-PCR assays**

The small nucleolar-RNAs (snoRNAs); RNU44 and RNU48, which were selected as internal controls, are commonly used for assessing miRNA expression, however do show variation in expression in different cancer types (Gee et al., 2011). In this study, some discrepancies in the efficiency of the RNU44 and RNU48 primers were observed, and this introduces some bias. Notably different Ct values for RNU44 were detected between D425 and the other cell lines. Subsequently, RNU48 was assessed as a control to be used in D425, and demonstrated similar efficiency to RNU44.

In subsequent post-transfection experiments, variation in RNU44/RNU48 expression was observed across all samples, which hints at a change induced by the transfection process or by miR-200b. Such variation was not expected when these internal control were selected, as previous analysis has demonstrated their validity (Genovesi, Anderson, Carter, Giles, & Dallas, 2012). Additionally, experimental error may be a factor, due to inexperience with the technique, or potentially the transfections themselves affect RNU44/RNU48 expression. Taking these possibilities into consideration, a range of potential internal controls should be assessed to reduce this variation.

Considering the consistent variation in internal control expression between cells that were transfected with mir-200b compared to those transfected the control, data was simply presented as  $2^{-\Delta Ct}$  (i.e. expression relative to control) and Log2 transformed, to avoid potential bias.

## **7.5 Additional considerations**

Although here it is proposed that DACH1 and miR-200b may be involved in Group 4 medulloblastoma pathogenesis, we were only able to test this association in Group 3 medulloblastoma cell lines. However, DACH1 up-regulation was detected in all medulloblastoma subgroups relative to normal cerebellum, suggesting that DACH1 overexpression may be relevant to medulloblastoma more generally. Taking this into consideration, it is possible that any association between DACH1 and miR-200b in medulloblastoma pathogenesis is not exclusive to Group 4. Indeed, we observed the inverse correlation in most of the cell lines including those of the SHH subgroup. Additionally, the roles of DACH1 and miR-200b in EMT raise the possibility that this putative association is relevant across all metastatic medulloblastoma, not just in Group 4.

## 8.0 CONCLUSION

The regulation of DACH1 by miR-200b remains to be definitively demonstrated. Although our findings were not suggestive of regulation at either the mRNA or protein level, initial correlative evidence would suggest an association. Additionally, our approach to assessing the functional relationship between DACH1 and miR-200b was limited due to both time constraints and issues with contaminated lentivirus requiring an alternative experimental approach. Considering all possibilities addressed above, the regulation of DACH1 is likely to be more complex, and probably involves additional microRNAs, particularly those of the miR-200 family with identical seed sequences to miR-200b (miR-200c and miR-429). If miR-200b does target DACH1, it may only produce a subtle change.

Cell lines stably transduced to express miR-200b could be used for long-term assessment of the effects of miR-200b not only on DACH1, but also the effects on cell phenotype, and particularly cell migration. Finally, although ambitious at this point, the development of mouse models engineered to over-express DACH1 and/or under-express miR-200b could potentially provide valuable understanding into the mechanisms of medulloblastoma pathogenesis.

Finally, although the role of DACH1 as an oncogene in medulloblastoma, remains to be conclusively demonstrated, the available data suggest that further characterisation of the role of DACH1 in medulloblastoma pathogenesis is warranted.

## 9.0 REFERENCES

- Atkins, M., Jiang, Y., Sansores-Garcia, L., Jusiak, B., Halder, G., & Mardon, G. (2013). Dynamic rewiring of the *Drosophila* retinal determination network switches its function from selector to differentiation. *PLoS genetics*, *9*(8).
- Bai, A. H. C., Bazhin, A. V., Eichmüller, S. B., Kulozik, A. E., Pscherer, A., Benner, A., . . . Jugold, M. (2012). MicroRNA-182 promotes leptomeningeal spread of non-sonic hedgehog-medulloblastoma. *Acta Neuropathologica*, *123*(4), 529-538.
- Barry, S. C., Bert, A. G., Farshid, G., Goodall, G. J., Gregory, P. A., Khew-Goodall, Y., . . . Vadas, M. A. (2008). The miR-200 family and miR-205 regulate epithelial to mesenchymal transition by targeting ZEB1 and SIP1. *Nature Cell Biology*, *10*.
- Cho, W. C. S. (2007). OncomiRs: the discovery and progress of microRNAs in cancers. *Molecular cancer*, *6*(1), 60-60.
- Cottonham, C. L., Kaneko, S., & Xu, L. (2010). miR-21 and miR-31 converge on TIAM1 to regulate migration and invasion of colon carcinoma cells. *The Journal of biological chemistry*, *285*(46), 35293-35302.
- D'Amato, N. C., Howe, E. N., & Richer, J. K. (2013). MicroRNA regulation of epithelial plasticity in cancer. *Cancer letters*, *341*(1), 46.
- Davalos, V., Moutinho, C., Villanueva, A., Boque, R., Silva, P., Carneiro, F., & Esteller, M. (2012). Dynamic epigenetic regulation of the microRNA-200 family mediates epithelial and mesenchymal transitions in human tumorigenesis. *Oncogene*, *31*(16), 2062-2074.
- Davis, R. J., Mardon, G., Shen, W., Sandler, Y. I., Amoui, M., Purcell, P., . . . Beaudet, A. L. (2001). Dach1 mutant mice bear no gross abnormalities in eye, limb, and brain development and exhibit postnatal lethality. *Molecular and cellular biology*, *21*(5), 1484-1490.
- Davis, R. J., Shen, W., Heanue, T. A., & Mardon, G. (1999). Mouse Dach, a homologue of *Drosophila* dachshund, is expressed in the developing retina, brain and limbs. *Development genes and evolution*, *209*(9), 526-536.
- Davis, R. J., Shen, W., Sandler, Y. I., Heanue, T. A., & Mardon, G. (2001). Characterization of mouse Dach2, a homologue of *Drosophila* dachshund. *Mechanisms of Development*, *102*(1-2), 169-179.

- Desmond, G. P., Gopal Krishna, R. D., Christophe, L., Tony, A., Hany, O. H., Ian, O. E., . . . Graham, R. B. (2014). DACH1: Its Role as a Classifier of Long Term Good Prognosis in Luminal Breast Cancer: e84428. *PLoS One* 9(1).
- DeSouza, R.-M., Jones, B. R. T., Lowis, S. P., & Kurian, K. M. (2014). Pediatric medulloblastoma - update on molecular classification driving targeted therapies. *Frontiers in oncology*, 4, 176.
- Ding, X.-M. (2014). MicroRNAs: regulators of cancer metastasis and epithelial-mesenchymal transition (EMT). *Chinese journal of cancer*, 33(3), 140-147.
- Djuranovic, S., Nahvi, A., & Green, R. (2012). miRNA-mediated gene silencing by translational repression followed by mRNA deadenylation and decay. *Science (New York, N.Y.)*, 336(6078), 237.
- Doench, J. G., & Sharp, P. A. (2004). Specificity of microRNA target selection in translational repression. *Genes & development*, 18(5), 504-511.
- Dubuc, A. M., Morrissy, A. S., Shih, D., Peacock, J., Ramaswamy, V., Rolider, A., . . . Unterberger, A. (2013). Aberrant patterns of H3K4 and H3K27 histone lysine methylation occur across subgroups in medulloblastoma. *Acta neuropathologica*, 125(3), 373-384.
- Esquela-Kerscher, A., & Slack, F. J. (2006). Oncomirs - microRNAs with a role in cancer. *Nature Reviews Cancer*, 6(4), 259-269.
- Fabbri, M., Croce, C. M., & Calin, G. A. (2008). MicroRNAs. *Cancer journal*, 14(1), 1-6.
- Feng, X., Wang, Z., Fillmore, R., & Xi, Y. (2014). MiR-200, a new star miRNA in human cancer. *Cancer letters*, 344(2), 166.
- Ferretti, E., Farcomeni, A., Nofroni, I., Laneve, P., Gioia, U., Caffarelli, E., . . . Giangaspero, F. (2009). MicroRNA profiling in human medulloblastoma. *International journal of cancer*, 124(3), 568-577.
- Finnegan, E. F., & Pasquinelli, A. E. (2013). MicroRNA biogenesis: regulating the regulators. *Critical Reviews in Biochemistry and Molecular Biology*, 48(1), 51-68.
- Friedman, H. S., et al., . (1988). Phenotypic and genotypic analysis of a human medulloblastoma cell line and transplantable xenograft (D341Med) demonstrating amplification of c-myc. *The American Journal of Pathology*, 130(3).
- Friedman, H. S., et al., (1985). Establishment and characterization of the human medulloblastoma cell line and transplantable xenograft D283 Medulloblastoma. *Journal of neuropathology and experimental neurology*, 44(6).

- Gee, H. E., Buffa, F. M., Camps, C., Ramachandran, A., Leek, R., Taylor, M., . . . Harris, A. L. (2011). The small-nucleolar RNAs commonly used for microRNA normalisation correlate with tumour pathology and prognosis. *Br J Cancer*, *104*(7), 1168-1177.
- Genovesi, L. A., Anderson, D., Carter, K. W., Giles, K. M., & Dallas, P. B. (2012). Identification of suitable endogenous control genes for microRNA expression profiling of childhood medulloblastoma and human neural stem cells. *BMC research notes*, *5*(1), 507-507.
- Genovesi, L. A., Carter, K. W., Gottardo, N. G., Giles, K. M., & Dallas, P. B. (2011). Integrated analysis of miRNA and mRNA expression in childhood medulloblastoma compared with neural stem cells. *PloS One*, *6*(9), e23935.
- Gerber, N. U., Mynarek, M., Von Hoff, K., Friedrich, C., Resch, A., & Rutkowski, S. (2014). Recent developments and current concepts in medulloblastoma. *Cancer Treatment Reviews*, *40*(3), 356-365.
- Gibson, P., Tong, Y., Robinson, G., Thompson, M. C., Currle, D. S., Eden, C., . . . Gilbertson, R. J. (2010). Subtypes of medulloblastoma have distinct developmental origins. *Nature*, *468*(7327), 1095-1099.
- Hailin, T., Min, D., Yunyun, T., Xinhua, X., Jiaoli, G., Yanan, K., . . . (2013). miR-200b and miR-200c as Prognostic Factors and Mediators of Gastric Cancer Cell Progression. *Clinical Cancer Research*, *19*(20).
- He, X. M., et al., (1991). Differentiation characteristics of newly established medulloblastoma cell lines (D384 Med, D425 Med, and D458 Med) and their transplantable xenografts. *Laboratory investigation; a journal of technical methods and pathology*, *64*(6).
- Holthouse, D. J., Dallas, P. B., Ford, J., Fabian, V., Murch, A. R., Watson, M., . . . Kees, U. (2008). Classic and desmoplastic medulloblastoma: complete case reports and characterizations of two new cell lines. *Neuropathology*, *29*(4).
- Hovestadt, V., Warnatz, H.-J., Ralser, M., Brun, S., Bunt, J., Jäger, N., . . . Ryzhova, M. (2014). Decoding the regulatory landscape of medulloblastoma using DNA methylation sequencing. *Nature*, *510*(7506), 537.
- Huang, Y., Yang, Y. B., Zhang, X. H., Yu, X. L., Wang, Z. B., & Cheng, X. C. (2013). MicroRNA-21 gene and cancer. *Medical oncology* *30*(1), 376-379.
- Huse, J. T., & Holland, E. C. (2010). Targeting brain cancer: advances in the molecular pathology of malignant glioma and medulloblastoma. *Nature reviews Cancer*, *10*(5), 319-331.

- Jacobsen, P. F., Jenken, D.J., Papadimitriou, J.M. . (1985). Establishment of a human medulloblastoma cell line and its heterotransplantation into nude mice. *Journal of neuropathology and experimental neurology*, 44(5), 472-485.
- Jones, D. T. W., Northcott, P. A., Kool, M., & Pfister, S. M. (2013). The role of chromatin remodeling in medulloblastoma. *Brain pathology*, 23(2), 193-199.
- Jones, D. T. W., Stütz, A. M., Rausch, T., Warnatz, H.-J., Ryzhova, M., Bender, S., . . . Lichter, P. (2012). Dissecting the genomic complexity underlying medulloblastoma. *Nature*, 488(7409), 100-105.
- Keles, G. E., et as., (1991). Establishment and characterisation of four human medulloblastoma-derived cell lines. *Oncology Research*, 7(10-11).
- Klesse, L. J., & Bowers, D. C. (2010). Childhood Medulloblastoma: Current Status of Biology and Treatment (Vol. 24, pp. 285-301). Cham: Adis International.
- Kong, Y. W., Ferland-McCollough, D., Jackson, T. J., & Bushell, M. (2012). microRNAs in cancer management. *The Lancet. Oncology*, 13(6), e249-e258.
- Korpak, M., Lee, E. S., Hu, G., & Kang, Y. (2008). The miR-200 family inhibits epithelial-mesenchymal transition and cancer cell migration by direct targeting of E-cadherin transcriptional repressors ZEB1 and ZEB2. *The Journal of Biological Chemistry*, 283(22), 14910-14914.
- Korshunov, A., Ryzhova, M., Cho, Y.-J., Wittmann, A., Benner, A., Weiss, W. A., . . . Jones, D. T. W. (2012). Biological and clinical heterogeneity of MYCN-amplified medulloblastoma. *Acta Neuropathologica*, 123(4), 515-527.
- Lau, J., Schmidt, C., Markant, S. L., Taylor, M. D., Wechsler-Reya, R. J., & Weiss, W. A. (2012). Matching mice to malignancy: molecular subgroups and models of medulloblastoma. *Child's nervous system: official journal of the International Society for Pediatric Neurosurgery*, 28(4), 521-532.
- Lee, J. W., Kim, H. S., Kim, S., Hwang, J., Kim, Y. H., Lim, G. Y., . . . Lee, S. (2012). DACH1 regulates cell cycle progression of myeloid cells through the control of cyclin D, Cdk 4/6 and p21Cip1. *Biochemical and Biophysical Research Communications*, 420(1), 91-95.
- Li, K. K. W., Lau, K. M., & Ng, H. K. (2013). Signaling pathway and molecular subgroups of medulloblastoma. *International journal of clinical and experimental pathology* 6(7), 1211.

- Li, L., Wang, D., Xue, M., Mi, X., Liang, Y., & Wang, P. (2014). 3' UTR shortening identifies high-risk cancers with targeted dysregulation of the ceRNA network. *Scientific Reports*, 4.
- Liang, F., Lu, Q., Sun, S., Zhou, J., Popov, V. M., Li, S., . . . Kong, B. (2012). Increased expression of dachshund homolog 1 in ovarian cancer as a predictor for poor outcome. *Int J Gynecol Cancer*, 22(3), 386-393.
- Lianoglou, S., Garg, V., Yang, J. L., Leslie, C. S., & Mayr, C. (2013). Ubiquitously transcribed genes use alternative polyadenylation to achieve tissue-specific expression. *Genes & development*, 27(21), 2380.
- Lindsey, J. C., Anderton, J. A., Lusher, M. E., & Clifford, S. C. (2005). Epigenetic events in medulloblastoma development. *Neurosurgery Focus*, 19(5), E10.
- Livak, K. J., & Schmittgen, T. D. (2001). Analysis of Relative Gene Expression Data Using Real-Time Quantitative PCR and the  $2^{-\Delta\Delta CT}$  Method. *Methods*, 25(4), 402-408.
- Ma, L., Young, J., Prabhala, H., Pan, E., Mestdagh, P., Muth, D., . . . Weinberg, R. A. (2010). miR-9, a MYC/MYCN-activated microRNA, regulates E-cadherin and cancer metastasis. *Nature Cell Biology*, 12(3), 247-256.
- MacDonald, T. J., Aguilera, D., & Castellino, R. C. (2014). The rationale for targeted therapies in medulloblastoma. *Neuro-oncology*, 16(1), 9-20.
- Mardon, G., Solomon, N. M., & Rubin, G. M. (1994). dachshund encodes a nuclear protein required for normal eye and leg development in Drosophila. *Development*, 120(12), 3473-3486.
- Men, D., Liang, Y., & Chen, L. (2014). Decreased expression of microRNA-200b is an independent unfavorable prognostic factor for glioma patients. *Cancer epidemiology* 38(2), 152.
- Min, H. S., Lee, J. Y., Kim, S.-K., & Park, S.-H. (2013). Genetic grouping of medulloblastomas by representative markers in pathologic diagnosis. *Translational Oncology* 6(3), 265.
- Nguyen, D. X., & Massagué, J. (2007). Genetic determinants of cancer metastasis. *Nature Reviews Genetics*, 8(5), 341-352.
- Northcott, P. A., Korshunov, A., Pfister, S. M., & Taylor, M. D. (2012). The clinical implications of medulloblastoma subgroups. *Nature reviews Neurology*, 8(6), 340.
- Northcott, P. A., Korshunov, A., Witt, H., Hielscher, T., Eberhart, C. G., Mack, S., . . . Taylor, M. D. (2011). Medulloblastoma comprises four distinct molecular variants. *Journal Of Clinical Oncology*, 29(11), 1408-1414.

- Northcott, P. A., Schumacher, S. E., Rubin, J. B., Beroukhi, R., Ellison, D. W., Marshall, C. R., . . . Leonard, J. R. (2012). Subgroup-specific structural variation across 1,000 medulloblastoma genomes. *Nature*, *488*(7409), 49-56.
- Northcott, P. A., Taylor, M. D., Pfister, S. M., Jones, D. T. W., Kool, M., Robinson, G. W., . . . Lichter, P. (2012). Medulloblastomics: the end of the beginning. *Nature reviews Cancer*, *12*(12), 818-834.
- Park, S.-M., Gaur, A. B., Lengyel, E., & Peter, M. E. (2008). The miR-200 family determines the epithelial phenotype of cancer cells by targeting the E-cadherin repressors ZEB1 and ZEB2. *Genes & development*, *22*(7), 894-907.
- Parsons, D. W., Bettegowda, C., Gallia, G. L., Jallo, G. I., Binder, Z. A., Nikolsky, Y., . . . Samayoa, J. (2011). The Genetic Landscape of the Childhood Cancer Medulloblastoma. *Science*, *331*(6016), 435-439.
- Pizer, B., & Clifford, S. (2008). Medulloblastoma: new insights into biology and treatment. *Archives of disease in childhood. Education and practice edition*, *93*(5), 137-144.
- Pöschl, J., Kool, M., Schüller, U., Stark, S., Neumann, P., Gröbner, S., . . . Pfister, S. M. (2014). Genomic and transcriptomic analyses match medulloblastoma mouse models to their human counterparts. *Acta neuropathologica*, *128*(1), 123-136.
- Remke, M., Ramaswamy, V., & Taylor, M. D. (2013). Medulloblastoma molecular dissection: the way toward targeted therapy. *Current Opinion In Oncology*, *25*(6), 674-681.
- Robinson, G., Zhu, X., Chalhoub, N., Baker, S. J., Huether, R., Kriwacki, R., . . . Wei, L. (2012). Novel mutations target distinct subgroups of medulloblastoma. *Nature*, *488*(7409), 43-48.
- Roussel, M. F., & Robinson, G. W. (2013). Role of MYC in Medulloblastoma. *Cold Spring Harbor Perspectives In Medicine*, *3*(11).
- Schmittgen, T. D., & Livak, K. J. (2008). Analyzing real-time PCR data by the comparative CT method. *Nat. Protocols*, *3*(6), 1101-1108.
- Schroeder, K., & Gururangan, S. (2014). Molecular variants and mutations in medulloblastoma. *Pharmacogenomics and Personalized Medicine*, *7*, 43-51.
- Selbach, M., Schwanhauss, B., & Thierfelder, N. (2008). Widespread changes in protein synthesis induced by microRNAs. *Nature* *455*, 58.
- Silber, J., Hashizume, R., Felix, T., Hariono, S., Yu, M., Berger, M. S., . . . Gupta, N. (2013). Expression of miR-124 inhibits growth of medulloblastoma cells. *Neuro-Oncology*, *15*(1), 83-90.

- Sunde, J., Donniger, H., Wu, K., Johnson, M., Pestell, R., Rose, G., . . . Birrer, M. (2006). Expression profiling identifies altered expression of genes that contribute to the inhibition of transforming growth factor-beta signaling in ovarian cancer. *Cancer Res*, 66(17), 8404 - 8412.
- Swartling, F. J., Yakovenko, S., Zhe, X.-N., Gilmer, H. C. F., Collins, R., Nagaoka, M., . . . Cancer och, v. (2010). Pleiotropic role for MYCN in medulloblastoma. *Genes & development*, 24(10), 1059-1072.
- Tavsanli, B. C., Ostrin, E. J., Burgess, H. K., Middlebrooks, B. W., Pham, T. A., & Mardon, G. (2004). Structure–function analysis of the Drosophila retinal determination protein Dachshund. *Developmental Biology*, 272(1), 231-247.
- Taylor, M. D., Gajjar, A., Ellison, D. W., Lichter, P., Gilbertson, R. J., Pomeroy, S. L., . . . Rutkowski, S. (2012). Molecular subgroups of medulloblastoma: the current consensus. *Acta Neuropathologica*, 123(4), 465-472.
- Thomson, D. W., Bracken, C. P., & Goodall, G. J. (2011). Experimental strategies for microRNA target identification. *Nucleic acids research*, 39(16), 6845-6853.
- Uziel, T., Hannon, G., Roussel, M. F., Karginov, F. V., Xie, S., Parker, J. S., . . . Gilbertson, R. J. (2009). The miR-17~92 cluster collaborates with the Sonic Hedgehog pathway in medulloblastoma. *Proceedings of the National Academy of Sciences* 106(8), 2812-2817.
- Vonlanthen, J., Marra, G., Okoniewski, M. J., Menigatti, M., Cattaneo, E., Pellegrini-Ochsner, D., . . . Buffoli, F. (2014). A comprehensive look at transcription factor gene expression changes in colorectal adenomas. *BMC cancer*, 14(1).
- Weeraratne, S. D., Bai, A. H. C., Warren, P., Pfister, S. M., Steen, J. A. J., Pomeroy, S. L., . . . Remke, M. (2012). Pleiotropic effects of miR-183~96~182 converge to regulate cell survival, proliferation and migration in medulloblastoma. *Acta Neuropathologica*, 123(4), 539-552.
- Williams, L. V., Veliceasa, D., Vinokour, E., & Volpert, O. V. (2013a). miR-200b inhibits prostate cancer EMT, growth and metastasis. *PloS one* 8(12).
- Williams, L. V., Veliceasa, D., Vinokour, E., & Volpert, O. V. (2013b). miR-200b inhibits prostate cancer EMT, growth and metastasis. *PloS one* 8(12)
- Wlodarski, P. K., & Jozwiak, J. (2008). Therapeutic targets for medulloblastoma. *Expert Opinion on Therapeutic Targets*, 12(4), 449-461.

- Wu, K., Chen, K., Wang, C., Jiao, X., Wang, L., Zhou, J., Wang, J., Li, Z., . . . Pestell, R. G. (2014). Cell fate factor DACH1 represses YB-1-mediated oncogenic transcription and translation. *Cancer Research*, 74(3), 829-839.
- Wu, K., Pestell, R. G., Katiyar, S., Li, A., Liu, M., Ju, X., . . . Casola, A. (2008). Dachshund inhibits oncogene-induced breast cancer cellular migration and invasion through suppression of interleukin-8. *Proceedings of the National Academy of Sciences of the United States of America*, 105(19), 6924-6929.
- Wu, K., Pestell, R. G., Liu, M., Li, A., Donninger, H., Rao, M., . . . Birrer, M. (2007). Cell fate determination factor DACH1 inhibits c-Jun-induced contact-independent growth. *Molecular Biology of the cell*, 18(3), 755-767.
- Wu, K., Sauter, G., Russell, R. G., Cvekl, A., Pestell, R. G., Li, A., . . . Lisanti, M. P. (2006). DACH1 is a cell fate determination factor that inhibits cyclin D1 and breast tumor growth. *Molecular and Cellular Biology*, 26(19), 7116-7129.
- Wu, L., Li, W., Guo, M., Herman, J. G., Brock, M. V., Wu, K., . . . Zhan, Q. (2014). Silencing DACH1 promotes esophageal cancer growth by inhibiting TGF- $\beta$  signaling. *PLoS ONE*, 9(4).
- Wu, L., Li, W., Guo, M., Herman, J. G., Brock, M. V., Wu, K., . . . Zhan, Q. (2014). Silencing DACH1 promotes esophageal cancer growth by inhibiting TGF- $\beta$  signaling. *PloS one* 9(4).
- Xu, Q.-F., Pan, Y.-W., Li, L.-C., Zhou, Z., Huang, Q.-L., Pang, J. C.-S., . . . Lv, S.-Q. (2014). MiR-22 is Frequently Down-regulated in Medulloblastomas, and Inhibits Cell Proliferation via the Novel Target PAPST1. *Brain Pathology*.
- Yan, W., Wu, K., Herman, J. G., Brock, M. V., Fuks, F., Yang, L., . . . Guo, M. (2013). Epigenetic regulation of *DACH1*, a novel Wnt signaling component in colorectal cancer. *Epigenetics*, 8(12), 1373-1383.
- Yan, W., Wu, K., Herman, J. G., Brock, M. V., Zhou, Y., Lu, Y., . . . Guo, M. (2014). Epigenetic silencing of DACH1 induces the invasion and metastasis of gastric cancer by activating TGF- $\beta$  signalling. *Journal of Cellular and Molecular Medicine*.
- Ye, F., Tang, H., Liu, Q., Xie, X., Wu, M., Liu, X., . . . Xie, X. (2014). miR-200b as a prognostic factor in breast cancer targets multiple members of RAB family. *Journal of translational medicine*, 12(1), 17-17.
- Zhang, J., & Ma, L. (2012). MicroRNA control of epithelial-mesenchymal transition and metastasis. *Cancer metastasis reviews*, 31(3-4), 653-662.

- Zhou, J., Tozeren, A., Zhao, K., Lisanti, M. p., Pestell, R. G., Wang. Chenguang., . . . Quong, A. (2010). Attenuation of Forkhead signaling by the retinal determination factor DACH1. *Proceedings of the National Academy of Sciences of the United States of America*, *107*(15), 6864-6869.
- Zhu, H., Guo, M., Wu, K., Yan, W., Hu, L., Yuan, J., . . . Yang, Y. (2013). Epigenetic silencing of DACH1 induces loss of transforming growth factor- $\beta$ 1 antiproliferative response in human hepatocellular carcinoma. *Hepatology (Baltimore, Md.)*, *58*(6), 2012-2022.
- Zhu, S., Wu, H., Wu, F., Nie, D., Sheng, S., & Mo, Y.-Y. (2008). MicroRNA-21 targets tumor suppressor genes in invasion and metastasis. *Cell Research*, *18*(3), 350-359.

## VII.

### APPENDICES

#### **Appendix A. Ethics approval declaration**

**Project Number: 11288 GEORGE**

**Project Name: The role of Dachshund Homolog 1 and the miR-200 family in medulloblastoma pathogenesis**

**Student Number: 10145031**

The ECU Human Research Ethics Committee (HREC) has reviewed your application and has granted ethics approval for your research project. In granting approval, the HREC has determined that the research project meets the requirements of the *National Statement on Ethical Conduct in Human Research*.

The approval period is from 16 May 2014 to 30 November 2014.

**Appendix B. qRT-PCR data**

Abbreviations	
Cycle Threshold	Ct
Standard Deviation	SD
$\Delta$ Ct	Normalised expression (Average Ct target – Average Ct internal control)
$\Delta\Delta$ Ct	Relative expression ( $\Delta$ Ct test – $\Delta$ Ct control)
Relative Quantitation	RQ

**qRT-PCR analysis of miR-200b in medulloblastoma cell lines**

	1	1	1	2	2	2	3	3	3	Average Ct	SD	Ct SD	$\Delta$ Ct	$\Delta\Delta$ Ct	$2^{-\Delta\Delta$ Ct}	Log2 RQ
<b>Daoy</b>																
<b>miR-200b</b>	29.33775	28.23541	27.96166	30.9249	30.3264		32.2878	30.77175	30.59115	30.054603	1.3612675	2.3718901	4.120265	-6.409015	84.977886	6.4090156
<b>RNU44</b>	27.03735	26.04543	25.43368	28.95017	28.47356		24.04086	23.79317	23.70048	25.934338	1.9423731					
<b>UW228</b>																
<b>miR-200b</b>	35	32.94062	32.02717	32.1551	31.09239		29.41409	29.85187		31.783034	1.7608922	1.8990813	7.1926971	-3.336583	10.102101	3.3365834
<b>RNU44</b>	25.649	24.34473	23.63739	25.61797	24.38796		24.00339	24.49192		24.590337	0.7111738					
<b>PER547</b>																
<b>miR-200b</b>	33.91859	33.03051	30.31595	36.436893	35.600822	30.62758	33.23739	34.47557	32.23739	33.28951	1.7537825	2.1293431	10.873032	0.3437517	0.7879895	-0.343751
<b>RNU44</b>	22.26352	21.78283	20.87944	22.123	22.156	20.60696	24.46166	23.82999	23.6449	22.416478	1.243004					
<b>D283</b>																
<b>miR-200b</b>	30.94545	30.12548	29.63841	34.11824	34.42992	33.86202	34.3392	33.8964	33.373714	32.747648	1.8253176	2.736219	10.529281	0	1	0
<b>RNU44</b>	25.96366	24.92622	23.86636	21.62347	20.97276	20.27967	21.67582	20.66049	19.996859	22.218368	2.0384087					
<b>D341</b>																
<b>miR-200b</b>	32.149	31.39827	30.14953	33.91484	33.7179	33.73136	34.83827	33.5502		33.328549	1.075924	1.7216024	10.832944	0.3036637	0.8101923	-0.303663
<b>RNU44</b>	24.77855	23.96069	22.82445	21.66571	20.61304	20.42971	21.72953	21.89726		22.495604	1.3439874					
<b>D425</b>																
<b>miR-200b</b>	32.95625	31.9533	33.25469	36.90059	31.45496	36.55563				33.269867	1.3609153	1.7390875	9.667665	-0.861615	1.817072	0.8616156
<b>RNU48</b>	24.50856	24.71615	24.80508	22.45871	22.39714	22.72757				23.602202	1.0827442					

qRT-PCR analysis of miR-200b expression in cell lines, 24 hours post-transfection with 20nM has-miR-200b-3p mimic/mRNA negative control #1, Log2 normalised to RNU44/RNU48

	1	1	1	2	2	2	Average	SD	Ct SD	$\Delta$ Ct	$2^{-\Delta$ Ct	Log2 RQ
<b><u>D341 mimic</u></b>												
<b>200b</b>	21.52807	21.48088	21.3638	24.9736	24.36937	24.28898	23.000792	1.55902	1.90097	-1.0367	2.05151	1.03668
<b>RNU44</b>	25.27176	25.13319	24.9591	22.9666	22.92638	22.96787	24.037475	1.08772				
<b><u>D341 control</u></b>												
<b>200b</b>	33.31676	32.99001	32.6836	34.3684	34.5461	33.86804	33.628817	0.68854	1.74598	9.33364	0.00155	-9.3336
<b>RNU44</b>	25.85066	25.87212	25.9705	22.8274	22.649	22.60136	24.295182	1.60448				
<b><u>D425 mimic</u></b>												
<b>200b</b>	22.76947	22.83269	22.8315	23.6105	23.57149	23.47665	23.182048	0.34584	0.4596	-2.0928	4.26572	2.09279
<b>RNU48</b>	24.97602	24.97247	24.9687	25.5533	25.59148	25.58709	25.274838	0.3027				
<b><u>D425 control</u></b>												
<b>200b</b>	32.67465	31.51094	32.6603	35.0083	35.07362		33.385556	1.41623	1.41769	8.37001	0.00302	-8.37
<b>RNU48</b>	24.9633	25.08756	24.9324	25.0912	25.00321		25.01555	0.06435				
<b><u>PER547 mimic</u></b>												
<b>200b</b>	21.57425	21.50414	21.4114	23.2451	23.20869	23.04483	22.331403	0.8384	1.68396	-1.6292	3.09342	1.6292
<b>RNU44</b>	25.53641	25.45538	25.2642	22.4639	22.52344	22.52037	23.960605	1.46041				
<b><u>PER547</u></b>												
<b>200b</b>	36.95118	36.41425	36.6832	36.9732	35.55816	35.30413	36.314012	0.65549	0.99237	11.6624	0.00031	-11.662
<b>RNU44</b>	25.4038	25.36094	25.4203	24.0012	23.86684	23.85657	24.651612	0.74507				
<b><u>D283 mimic</u></b>												
<b>200b</b>	22.22203	22.17984	22.1515	23.0709	23.03091		22.531016	0.42525	1.34479	-1.844	3.59014	1.84404
<b>RNU44</b>	25.41844	25.40425	25.4272	22.8376	22.78781		24.375056	1.27578				
<b><u>D283 control</u></b>												
<b>200b</b>	32.9179	33.74686	33.7841	35.1563	35.45034	34.59473	34.275028	0.87768	1.52129	9.28157	0.00161	-9.2816
<b>RNU44</b>	26.26553	26.256	26.1745	23.9212	23.75376	23.58982	24.99346	1.24257				

qRT-PCR analysis of miR-200b expression in cell lines, 48 hours post-transfection with 20nM has-miR-200b-3p mimic/mRNA negative control #1, Log2 normalised to RNU44/RNU48

	1	1	1	2	2	2	Average	SD	Ct SD	$\Delta$ Ct	$2^{-\Delta$ Ct	Log2 RQ
<b>D341 mimic</b>												
<b>200b</b>	24.552967	23.854042	23.599588	24.972551	24.921453	24.914639	24.46920667	0.547413953	0.574	2.705776333	0.153278119	-2.705776333
<b>RNU44</b>	21.538748	21.803959	21.522717	21.888258	21.977558	21.849342	21.76343033	0.172665887				
<b>D341 control</b>												
<b>200b</b>	34.174767		33.07282	34.115894	33.657753	33.456047	33.6954562	0.413018382	0.779176	10.3641804	0.000758701	-10.3641804
<b>RNU44</b>	22.542562		22.510897	23.98059	23.759356	23.862974	23.3312758	0.660704987				
<b>D425 mimic</b>												
<b>200b</b>	26.116674	26.044378	26.088703	24.615269	24.326649	24.432652	25.27072083	0.817162275	0.827505	0.2459315	0.843271148	-0.074032758
<b>RNU48</b>	25.216892	25.094225	25.117048	24.979593	24.903418	24.83756	25.02478933	0.130425547				
<b>D425 control</b>												
<b>200b</b>	34.248333	34.372295	34.1505	33.76569	34.66682	33.299202	34.08380667	0.441861531	0.493221	9.328851833	0.001555019	-9.328851833
<b>RNU48</b>	24.608341	24.972895	24.366798	24.999498	24.735964	24.846233	24.75495483	0.219147201				
<b>PER547 mimic</b>												
<b>200b</b>	21.938042	22.042686	22.033072	25.474108	25.3925		23.3760816	1.680311545	1.720426	1.1938188	0.437144211	-1.1938188
<b>RNU44</b>	22.827246	21.958355	21.736357	22.10297	22.286386		22.1822628	0.369350512				
<b>PER547 control</b>												
<b>200b</b>	36.95305	37.725636	36.3772	35.42836	34.3852	35.96322	36.13877767	1.068375121	2.170457	12.18951917	0.000214086	-12.18951917
<b>RNU44</b>	22.153275	22.079008	21.961515	25.992462	25.910704	25.598587	23.9492585	1.889301078				
<b>D283 mimic</b>												
<b>200b</b>	25.095387	25.30452	25.715897	25.835491	25.698816	25.5942	25.5407185	0.258051448	0.456851	1.740204833	0.299327175	-1.740204833
<b>RNU44</b>	23.887083	24.141254	24.051447	22.99429	23.801323	23.927685	23.80051367	0.376991504				
<b>D283 control</b>												
<b>200b</b>	36.616478	0	36.453217	33.53491	32.781097	32.351334	34.3474072	2.042113168	2.230966	10.5703502	0.000657669	-10.5703502
<b>RNU44</b>	22.72779		22.627365	24.514252	24.520742	24.495136	23.777057	0.898322239				

qRT-PCR analysis of miR-200b expression in cell lines, 24 hours post-transfection with 50nM has-miR-200b-3p mimic/mRNA negative control #1, Log2 normalised to RNU44/RNU48

	1	1	1	2	2	2	Average	SD	Ct SD	$\Delta$ Ct	$2^{-\Delta$ Ct	Log2 RQ
<b>D341 mimic</b>												
<b>200b</b>	21.70596	21.71921	21.4992	21.0093	21.00304	24.07897	21.83594667	1.045000335	1.540448	-0.46181	1.377268651	0.46181
<b>RNU44</b>	21.30863	21.16586	21.03312	23.4757	23.43556	23.36767	22.29775667	1.131792751				
<b>D341 control</b>												
<b>200b</b>	31.64931	31.72205	31.58662	31.64931	31.72205	31.58662	31.65266	0.055339787	0.087961	7.27798	0.00644332	-7.27798
<b>RNU44</b>	24.47125	24.3222	24.33059	24.47125	24.3222	24.33059	24.37468	0.068371152				
<b>D425 mimic</b>												
<b>200b</b>	25.96286	25.49348	25.42987	22.06564	21.67721	31.76428	25.286096	3.311787449	3.339333	-0.093160667	1.066704568	0.093160667
<b>RNU48</b>	25.83469	25.7955	25.78981	24.95746	24.98006	24.91802	25.37925667	0.428026818				
<b>D425 control</b>												
<b>200b</b>	32.17822	31.98237	31.8603	32.17822	31.98237	31.8603	32.00696333	0.130950132	0.138942	7.06575	0.007464441	-7.06575
<b>RNU48</b>	24.97568	24.87556	24.9724	24.97568	24.87556	24.9724	24.94121333	0.046443225				
<b>PER547 mimic</b>												
<b>200b</b>	21.48369	21.45464	21.48848	21.64073	21.45058	21.31722	21.47255667	0.094510347	0.537933	-1.36995	2.584616084	1.36995
<b>RNU44</b>	22.37408	22.26259	22.3184	23.46352	23.40174	23.23471	22.84250667	0.529565485				
<b>PER547 control</b>												
<b>200b</b>	32.83283	32.98308	33.08717	32.83283	32.98308	33.08717	32.96769333	0.104402334	0.125423	8.09478	0.003657871	-8.09478
<b>RNU44</b>	24.96535	24.85565	24.79774	24.96535	24.85565	24.79774	24.87291333	0.06950681				
<b>D283 mimic</b>												
<b>200b</b>	22.76589	22.880306	22.77436	21.13978	20.98208	21.03628	21.92978267	0.879059396	0.891459	-0.994464	1.99234018	0.994464
<b>RNU44</b>	23.01532	23.09686	23.04672	22.93132	22.75279	22.70247	22.92424667	0.148167553				
<b>D283 control</b>												
<b>200b</b>	32.44007	32.6546	32.32044	32.44007	32.6546	32.32044	32.47170333	0.138241883	0.147225	8.792446667	0.002255329	-8.792446667
<b>RNU44</b>	23.73654	23.68784	23.61339	23.73654	23.68784	23.61339	23.67925667	0.050640799				

qRT-PCR analysis of DACH1 expression in cell lines, Log2 normalised to GAPDH, relative to D283

	1	1	1	1	2	2	2	3	3	Average Ct	Standard Deviation	Ct SD	ΔCt	ΔΔCt	2 <sup>-ΔΔCt</sup>	Log2 RQ
<b>Daoy</b>																
DACH1	32.94137	33.04392	33.36116	33.56143	35	35		32.31932	32.52079	33.468499	0.960992	1.5634146	18.667709	9.8798465	0.0010614	-9.879846
GAPDH	13.49108	13.79862	13.979	14.14775	16.819	16.853		14.55992	14.75795	14.80079	1.2331908					
<b>UW228</b>																
DACH1	27.7054	27.8913	28.35166	28.48279	22.28466	27.26823	27.03695	29.44535	28.09034	27.395187	1.9260906	2.4187078	10.980673	2.1928111	0.2187248	-2.192811
GAPDH	14.57776	14.75679	14.78471	15.13801	17.35307	17.8131	17.76897	18.27613	17.26208	16.414513	1.4629841					
<b>PER547</b>																
DACH1	22.71583	22.69571	22.78952	22.88313	21.56316	21.38265	21.66921	19.97557		21.959348	0.9464508	1.4715609	5.1282463	-3.659616	12.637297	3.659616
GAPDH	15.87293	15.81801	15.89992	15.96786	18.2921	18.41454	18.11345	16.27		16.831101	1.1268196					
<b>D283</b>																
DACH1	27.27899	27.72077	27.85543	27.92399	25.00596	24.94711	24.89661	25.77412	24.47594	26.208769	1.3758596	1.7212747	8.7878622	0	1	0
GAPDH	16.45743	16.48814	16.53477	16.64414	18.21558	18.29747	18.98769	18.7073	16.45564	17.420907	1.0343099					
<b>D341</b>																
DACH1	23.22119	23.27677	23.29145	23.23901	25.99904	22.20039				23.537975	1.1665269	1.2683836	6.9259158	-1.861946	3.6349774	1.8619464
GAPDH	15.93585	16.08492	16.5373	16.69411	17.32265	17.097525				16.612059	0.4980081					
<b>D425</b>																
DACH1	23.57904	23.52437	23.02143	23.00439	25.05538	24.94749				23.85535	0.8404654	1.5976112	7.9584917	-0.829370	1.7769099	0.8293706
GAPDH	15.46338	15.1391	14.7202	14.6054	18.25849	17.19458				15.896858	1.3586682					

qRT-PCR analysis of DACH1 expression in cell lines, 24 hours post-transfection with 20nM has-miR-200b-3p mimic/mRNA negative control #1, Log2 normalised to GAPDH

	1	1	1	2	2	2	Average	SD	Ct SD	ΔCt	2 <sup>ΔCt</sup>	Log2 RQ
<b><u>D341 mimic</u></b>												
<b>DACH1</b>	23.91269	23.88669	23.8998	24.35321	24.4582	24.71346	24.2040083	0.3226235	0.591888	5.98396033	63.29239841	5.983960333
<b>GAPDH</b>	18.77639	18.81374	18.85933	17.68149	17.83187	17.95116	18.220048	0.4962309				
<b><u>D425mimic</u></b>												
<b>DACH1</b>	28.29979	28.23658	28.35454	27.10415	27.33318	27.45576	27.79733333	0.51128814	0.880431	9.164265	573.7446557	9.164265
<b>GAPDH</b>	19.59138	19.55558	19.09992	17.73256	17.83134	17.98763	18.6330683	0.80183266				
<b><u>PER547 mimic</u></b>												
<b>DACH1</b>	23.73677	23.70025	23.74679	23.78208	23.87966	23.93569	23.7968733	0.08346592	0.175963	5.62017167	49.18585809	5.620171667
<b>GAPDH</b>	18.35739	18.32396	18.35612	18.0478	17.99704	17.9779	18.1767017	0.17075337				
<b><u>D283 mimic</u></b>												
<b>DACH1</b>	27.80856	27.76054	27.87219	27.3417	27.54622		27.665842	0.19559811	0.602938	9.620732	787.2794443	9.620732
<b>GAPDH</b>	18.5109	18.55209	18.46779	17.34076	17.35401		18.04511	0.57032895				
<b><u>D341 control</u></b>												
<b>DACH1</b>	23.13936	23.17296	23.19764	26.62645	26.53385	26.42056	24.84847	1.67962377	1.558344	7.015495	129.3821696	7.015495
<b>GAPDH</b>	17.75568	17.98409	17.99052	17.75189	17.73875	17.77692	17.832975	0.10971628				
<b><u>D425 control</u></b>												
<b>DACH1</b>	27.90295	27.94307	27.7853	26.47859	26.44867	26.58408	27.1904433	0.68951752	0.898571	8.78111333	439.9248642	8.781113333
<b>GAPDH</b>	19.05323	19.1196	19.09992	17.66661	17.71298	17.80364	18.40933	0.68305709				
<b><u>PER547</u></b>												
<b>DACH1</b>	22.9135	22.91904	22.9501	23.61335	23.67364	23.62402	23.282275	0.3553969	0.7277777	5.54459167	46.67543836	5.544591667
<b>GAPDH</b>	18.46054	18.40936	18.44321	17.07402	16.96351	17.07546	17.7376833	0.7011624				
<b><u>D283 control</u></b>												
<b>DACH1</b>	27.55064	27.59835	27.561	27.86538		27.93596	27.702266	0.1291298	0.454163	9.450232	699.5250931	9.450232
<b>GAPDH</b>	18.58314	18.60515	18.60237	17.68924		17.78027	18.252034	0.39311391				

qRT-PCR analysis of DACH1 expression in cell lines, 48 hours post-transfection with 20nM has-miR-200b-3p mimic/mRNA negative control #1, Log2 normalised to GAPDH

	1	1	1	2	2	2	Average	SD	Ct SD	$\Delta$ Ct	$2^{\Delta}$ Ct	Log2 RQ
<b>D341 mimic</b>												
<b>DACH1</b>	23.299927	23.431452	23.508732	24.93911	24.966257	24.952692	24.18302833	0.772107428	1.119886	4.71537483	26.27055607	4.715374833
<b>GAPDH</b>	18.943432	18.579432	18.484972	20.317513	20.274754	20.205818	19.4676535	0.81116868				
<b>D341 control</b>												
<b>DACH1</b>	23.952806	23.958572	24.042336	23.884453	23.878902	23.847736	23.9274675	0.065025981	0.132252	4.89886767	29.83363091	4.898867667
<b>GAPDH</b>	19.24158	18.916302	18.899393	19.045921	19.081867	18.986536	19.02859983	0.115161148				
<b>D425mimic</b>												
<b>DACH1</b>	26.06653	26.27913	26.442982	27.98095	27.969145	27.992262	27.12183317	27.12183317	1.111041	7.89874633	238.6489756	7.898746333
<b>GAPDH</b>	18.508165	18.52896	18.544676	19.878576	19.944468	19.933676	19.22308683	19.22308683				
<b>D425 control</b>												
<b>DACH1</b>	25.4806	25.741081	25.930473	27.702425	27.660604	27.638617	26.6923	0.983776386	-1.153707	7.395872	168.4144363	7.395872
<b>GAPDH</b>	18.817703	18.719215	18.566668	19.944006	19.958818	19.772158	19.296428	0.602679979				
<b>PER547 mimic</b>												
<b>DACH1</b>	22.879507	22.907139	22.927818	22.686193	22.721674	22.697565	22.803316	22.803316	0.541169	4.62042033	24.59716831	4.620420333
<b>GAPDH</b>	17.54823	17.87284	17.635185	18.55324	18.996838	18.491041	18.18289567	18.18289567				
<b>PER547 control</b>												
<b>DACH1</b>	22.501484	22.606667	22.935978	23.2088	23.197466	23.114368	22.9274605	0.280305278	0.555234	4.64546233	25.02784785	4.645462333
<b>GAPDH</b>	17.891216	17.81557	17.711107	18.742556	18.796707	18.734833	18.28199817	0.479284319				
<b>D283 mimic</b>												
<b>DACH1</b>	26.19131	26.163534	26.210775	27.599478	27.612772	27.557426	26.88921583	0.701008718	0.775911	8.18087533	290.1942922	8.180875333
<b>GAPDH</b>	18.35787	18.43601	18.344559	19.11062	19.031214	18.96977	18.7083405	0.332603851				
<b>D283 control</b>												
<b>DACH1</b>	26.738604	26.66084	26.774017	27.350254	27.338509	27.33284	27.03251067	0.309874357	0.319274	8.71453267	420.0836037	8.714532667
<b>GAPDH</b>	18.409344	18.323383	18.221207				18.317978	0.076901639				

qRT-PCR analysis of DACH1 expression in cell lines, 24 hours post-transfection with 50nM has-miR-200b-3p mimic/mRNA negative control #1, Log2 normalised to GAPDH

	1	1	1	2	2	2	Average	SD	Ct SD	$\Delta$ Ct	$2^{\Delta}$ Ct	Log2 RQ
<b><u>D341 mimic</u></b>												
DACH1	23.17405	23.12604	22.91455	23.75813	23.58543	23.6579	23.36935	0.312326337	1.032196333	5.409946667	42.51637428	5.409946667
GAPDH	17.06121	16.82255	17.05308	18.94008	18.97713	18.90237	17.95940333	0.983809702				
<b><u>D341 control</u></b>												
DACH1	25.29235	25.63156	25.59295	25.29235	25.63156	25.59295	25.50562	0.151626191	0.155278891	6.102083333	68.69262606	6.102083333
GAPDH	19.44129	19.40941	19.35991	19.44129	19.40941	19.35991	19.40353667	0.033481817				
<b><u>D425mimic</u></b>												
DACH1	27.1276	27.08355	27.03174	28.37879	28.3133	28.36819	27.717195	0.637157805	0.707991419	8.36563	329.8417019	8.36563
GAPDH	19.07971	19.09004	18.97393	19.72562	19.58329	19.6568	19.351565	0.30867747				
<b><u>D425 control</u></b>												
DACH1	28.78645	28.58378	28.47351	28.78645	28.58378	28.47351	28.61458	0.12960026	0.153605192	9.209646667	592.0793251	9.209646667
GAPDH	19.51728	19.3758	19.32172	19.51728	19.3758	19.32172	19.40493333	0.082451973				
<b><u>PER547 mimic</u></b>												
DACH1	24.11801	24.12504	23.8416	23.21038	23.19758	23.17419	23.61113333	0.427529331	0.51569891	4.771745	27.31733803	4.771745
GAPDH	18.67534	18.63002	18.39411	19.14321	19.14737	19.04628	18.83938833	0.288381756				
<b><u>PER547 control</u></b>												
DACH1	25.51031	25.60321	25.27715	25.51031	25.60321	25.27715	25.46355667	0.137157298	0.156392311	5.149146667	35.4852279	5.149146667
GAPDH	20.36198	20.37292	20.20833	20.36198	20.37292	20.20833	20.31441	0.075142734				
<b><u>D283 mimic</u></b>												
DACH1	28.02566	27.97278	27.91611	27.92245	28.01564	27.60113	27.90896167	0.143796683	0.383694633	9.079776667	541.109465	9.079776667
GAPDH	18.50107	18.52217	18.41807	19.29328	19.16208	19.07844	18.829185	0.355730355				
<b><u>D283 control</u></b>												
DACH1	29.96095	29.90553	29.79715	29.96095	29.90553	29.79715	29.88787667	0.068026172	0.076160602	9.954003333	991.8673175	9.954003333
GAPDH	19.96734	19.88682	19.94746	19.96734	19.88682	19.94746	19.93387333	0.034247294				